



Review

Luminescent graphene quantum dots as new fluorescent materials for environmental and biological applications

Liping Lin^a, Mingcong Rong^a, Feng Luo^c, Dongmei Chen^c, Yiru Wang^a, Xi Chen^{a,b,*}

^a Department of Chemistry and the MOE Key Laboratory of Spectrochemical Analysis & Instrumentation, College of Chemistry and Chemical Engineering, Xiamen University, Xiamen 361005, China

^b State Key Laboratory of Marine Environmental Science, Xiamen University, Xiamen 361005, China

^c Fujian Research Institute of Metric Science, Fuzhou 350003, China

ARTICLE INFO

Keywords:

Biological application
Chemical properties
Cytotoxicity
Environmental application
Fluorescent material
Graphene quantum dot
Luminescent graphene quantum dot
Physical properties
Size-tuning method
Surface-chemistry method

ABSTRACT

Luminescent graphene quantum dots (GQDs) have attracted tremendous attention from the scientists in chemistry, materials science, physics and biology, because of their superiority of good stability, excellent optical and electrochemical properties, resistance to photobleaching and low cytotoxicity. We summarize the recent advances in the preparation and the properties of GQDs and their applications in environmental and biological areas. In addition, we discuss the future development of GQDs.

© 2013 Elsevier Ltd. All rights reserved.

Contents

1. Introduction	84
2. Approaches to synthesis	84
2.1. Size-tuning approaches	84
2.1.1. Top-down methods	84
2.1.2. Bottom-up approaches	87
2.2. Surface chemistry-tuned strategies	89
2.2.1. Surface functionalization	89
2.2.2. Doping with other elements	91
3. Physical and chemical properties	92
3.1. Optical properties	92
3.1.1. Absorbance and PL	92
3.1.2. Upconverted PL	93
3.2. Cytotoxicity	93
3.3. Electrocatalytic activity	94
3.4. Electrochemiluminescence	94
4. Applications	96
4.1. Environmental	96
4.2. Bioanalytical	97
4.2.1. Detection of biological molecules	97
4.2.2. Drug release	99
4.2.3. DNA cleavage	99
4.2.4. Bioimaging	100

* Corresponding author at: Department of Chemistry and the MOE Key Laboratory of Spectrochemical Analysis & Instrumentation, College of Chemistry and Chemical Engineering, Xiamen University, Xiamen 361005, China.

E-mail address: xichen@xmu.edu.cn (X. Chen).

5. Summary and outlook	100
Acknowledgments	100
References	100

1. Introduction

Carbon-based nanomaterials, known for their different morphologies and unique properties, have inspired intensive research efforts over the past few decades. Since zero-dimensional fullerene [1,2], one-dimensional carbon nanotubes (CNTs) [3–5] and two-dimensional graphene [6,7] have been discovered in succession, they have been applied in the biological, chemical, material and environmental fields. Graphene, a novel single-atom-thick and two-dimensional nano graphitic carbon sheet, exhibits characteristics including large surface area, high carrier transport mobility, superior mechanical flexibility and excellent thermal and chemical stability, which are suitable for various applications in optoelectronic devices, energy-storage media and drug-delivery vehicles [8–10]. In addition to the superlative electronic properties, recent theoretical and experimental studies show that the distinctive properties of graphene can be realized by tuning the band gap of graphene via altering their size, destroying the integrity of the π system and controlling the chemical structures or layers of graphene [11–14]. Consequently, graphene quantum dots (GQDs) were discovered very recently as a class of zero-dimensional graphitic nanomaterials with lateral dimensions less than 100 nm in single layer, double layers and a few layers (3 to <10) [15–17]. They are superior in terms of chemical inertness, ease of production, resistance to photobleaching, low cytotoxicity and excellent biocompatibility in comparison to conventional semiconductor QDs, thus making them promising in sensors, bioimaging, optoelectronic devices and so on [18,19]. Moreover, similar to graphene, GQDs have excellent characteristics of large surface area, large diameter, fine surface grafting using the π - π conjugated network or surface groups and other special physical properties. Furthermore, the carboxyl and hydroxyl groups at their edge enable them to display excellent water solubility and suitability for successive functionalization with various organic, inorganic, polymeric or biological species [20–23].

In this article, we aim to review the recent development of a protocol and a methodology for the preparation of GQDs and their applications based on their excellent properties. We summarize the currently available approaches to the preparation of GQDs, and reveal their characteristics associated with their size, shape, doping, surface modification, and reaction to pH and solvents. Subsequently, we describe the applications of GQDs in environmental and biological fields. In addition, we speculate on some critical issues for further exploration and possible ongoing developments of GQDs.

2. Approaches to synthesis

So far, the synthesis of GQDs with excellent photoluminescence (PL) properties can be divided into two strategies: size tuning and surface chemistry. Approaches to size tuning can generally be classified into top-down and bottom-up methods. Top-down methods include cutting large graphene-based materials into nanosized GQDs. But, bottom-up approaches involve preparing GQDs with organic molecules as a carbon source. Surface chemistry-tuned strategies include surface functionalization [20–24] and doping other elements [25–28].

2.1. Size-tuning approaches

In general, the optical properties of GQDs greatly depend on their size due to the quantum-confinement effect, and the variation in density and nature of sp^2 sites available in GQDs. Thus, the energy band gap of GQDs can be tuned by changing their size.

2.1.1. Top-down methods

2.1.1.1. Surface-catalyzed decomposition of C_{60} . In view of the flexible structural transition between graphene and fullerenes, geometrically well-defined GQDs were successfully synthesized through the ruthenium (Ru)-catalyzed cage-opening of C_{60} [29]. The strong C_{60} -Ru interaction ensures the embedding of C_{60} molecules on the surface and the fragmentation of the embedded molecules at elevated temperatures, and then the carbon clusters obtained undergo diffusion and aggregation to form GQDs on the Ru (0001) substrate. By controlling the annealing temperature and the density of the carbon clusters, the equilibrium shape of the graphene can be tailored.

2.1.1.2. Acidic exfoliation and oxidation. Several reports reveal that acidic exfoliation and oxidation is an effective way to prepare GQDs. And they have been obtained on a large scale via acid treatment and chemical exfoliation of traditional μm -sized pitch-based carbon fiber (CF) (Fig. 1) [30]. The size of these GQDs varies with the reaction temperature (80°C, 100°C and 120°C) in the ranges 1–4 nm, 4–7 nm and 7–11 nm, resulting in the emission color (blue, green and yellow), and the band gap of GQDs can be tailored accordingly. Similarly, multi-layer graphene is exfoliated from CF with bath sonication for 1 h at 50–60°C and treatment of the solution with a mixture of H_2SO_4 and HNO_3 to form different colored photoluminescent GQDs (blue, green, yellow, red and near-IR) [31]. Recently, single-layer and multi-layer GQDs (1–3 nm in thick-

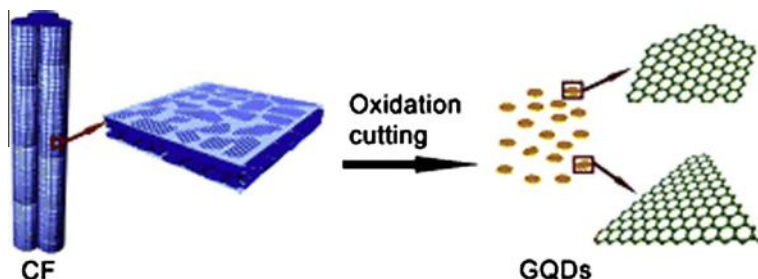


Fig. 1. Carbon-fiber (CF) oxidation cutting into graphene quantum dots (GQDs) [30].

ness) were prepared simultaneously from XC-72 carbon black by refluxing with concentrated HNO_3 [32]. The resultant solution was further separated by centrifuging in acidic solution. The supernatant and the sediment exhibit green or yellow under excitation at 365 nm, respectively. The PL properties of the GQDs obtained mainly lie on the zig-zag edges of the graphene. All this work shows that acidic exfoliation and oxidation is superior in ease of production, low cost, high yield and mass production, although there are still some disadvantages, such as harsh conditions, elimination of excess acid used in the process and the time needed.

2.1.1.3. Electrochemical oxidation. As a green, easy and scalable approach to synthesis, electrochemical oxidation effectively avoids the use of excessively strong acid and complicated purification and separation procedures. GQDs are obtained from a graphite electrode via ionic liquid-assisted electrochemical exfoliation based on the reaction between anodic oxidation of water and anionic intercalation from the ionic liquid (Fig. 2) [33]. In this process, a water-miscible ionic liquid, 1-butyl-3-methylimidazolium tetrafluoroborate $[\text{BMI}_m][\text{BF}_4]$, mixed with water at different fractions, is used as an electrolyte for the electrochemical exfoliation of graphite. Higher water content lowers electrolyte resistance and narrows the electrochemical potential window. Meanwhile, the chemical composition and the surface passivation of the exfoliated GQDs varies with the change in the ratio of the ionic liquid to water in the electrolyte.

Using electrochemical exfoliation of graphite by reduction with hydrazine without adding any polymeric or surfactant stabilizers at room temperature, water-soluble, uniform GQDs with strong yellow emission with a quantum yield of 14% are synthesized. Study of the structure and emission mechanism of the GQDs demonstrated that the PL results from the abundant phthalhydrazide-like groups and hydrazide groups at the edge of the graphene. More importantly, this approach enables large-scale production of an aqueous solution of GQDs.

An electrochemical preparation of GQDs with smooth edges and fewer defects in a uniform size of 3 nm, 5 nm and $8.2 (\pm 0.3)$ nm from multi-walled CNTs (MWCNTs) was reported (Fig. 3) [34]. The preparation carried out in propylene carbonate using LiClO_4 at both 90°C and 30°C had quantum yields of 6.3% and 5.1%, respectively.

Experimental results also proved that the PL properties of GQDs can be tailored by size variation via changing the diameter of the CNTs, the electric field, the concentration of supporting electrolyte and the temperature. The study on the effect of media, anion and solvent revealed that cation/propylene carbonate complexes were primarily responsible for the high-yield exfoliation of oxidized MWCNTs to produce GQDs.

2.1.1.4. Hydrothermal and solvothermal cutting. Graphene oxide (GO) sheets treated using thermal reduction result in micrometer-sized rippled graphene sheets (GSs), which can then be used as starting material to prepare functionalized GQDs with sub-10 nm size via the hydrothermal approach (Fig. 4) [15]. The bright blue emission of the as-prepared GQDs directly was induced by the formation of free zig-zag sites under hydrothermal conditions. In 2011, GQDs were obtained on a large scale with a quantum yield of 11.4% when treating GO via a one-step solvothermal route [35]. The GQDs of 5.3 nm size and 1.2 nm height display strongly green PL derived from the surface effect. These GQDs can be dissolved in water and most polar organic solvents without further chemical modifications.

2.1.1.5. Microwave and ultrasonic shearing. As high-energy technology, microwave and ultrasonic shearing is capable of cutting large graphene-based material into GQDs, which effectively shortens the synthesis time. GQDs are prepared with a mixture of GO aqueous solution, HNO_3 (65%) and H_2SO_4 (98%) using the microwave-hydrothermal protocol [36]. The resultant product exhibits an unusual emission transformation in strong acidic media and at high concentration, induced by self-assembled J-type aggregation under restrained π - π interactions.

As shown in Fig. 5, two-color GQDs via cleaving GO under acid conditions are also prepared using microwave irradiation [37]. The cleaving and reduction processes are accomplished simultaneously using microwave treatment without an additional reducing agent. The greenish-yellow GQDs (gGQDs) are further reduced with NaBH_4 to obtain bright blue luminescent GQDs (bGQDs) with a quantum yield as high as 22.9%. The PL behavior is ascribed to the transition from the lowest unoccupied molecular orbital to the highest occupied molecular orbital with a carbene-like triplet ground state.

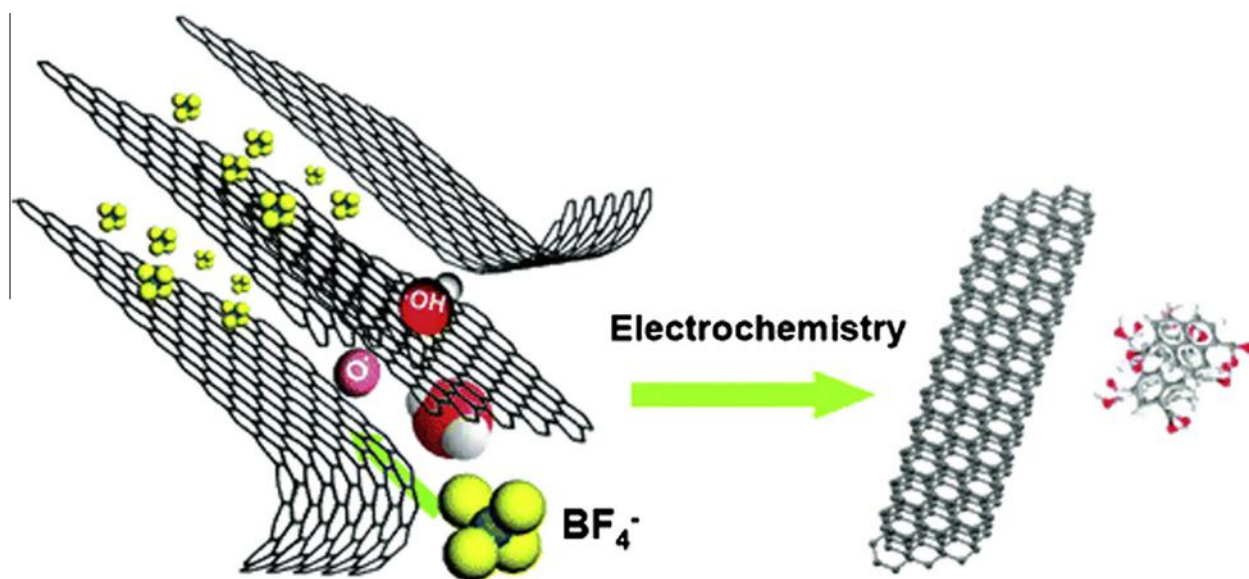


Fig. 2. The exfoliation process showing the attack of the graphite edge planes by hydroxyl and oxygen radicals, which facilitated the intercalation of BF_4^- anions [33].

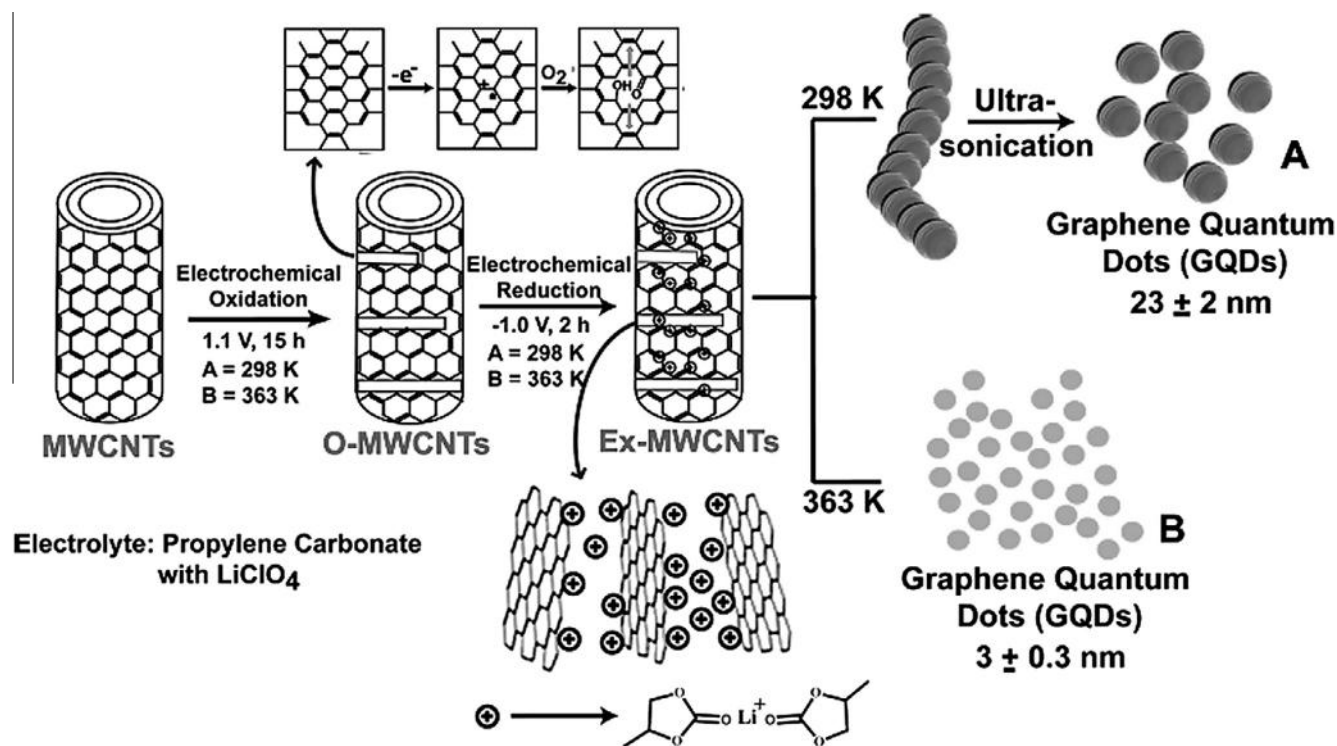


Fig. 3. The various processing stages involved in the preparation of photoluminescent graphene quantum dots (GQDs) from multi-walled carbon nanotubes (MWCNTs) using the electrochemical approach [34].

Water-soluble GQDs with a size around 20 nm and a monolayer thickness are prepared by exfoliating and disintegrating MWCNTs and graphite flakes [38]. In the process, potassium-graphite intercalation compounds (K-GIC) are formed by intercalating K atoms between the covalently-bonded GSs in the MWCNTs via the weak interlayer van der Waals force (Fig. 6). The hydrogen gas generated in the reaction between K-GIC and EtOH can simultaneously exfoliate the thin graphite sheets. Short exposure of the K-GICs to air results in many defects on the graphene walls; however, using ultrasonication, K-GICs kept on reacting violently with EtOH-H₂O to exfoliate and to disintegrate the walls of the MWCNTs to yield monolayered GQDs.

2.1.1.6. Other chemical methods. Given the emerging properties and ongoing applications of GQDs, their preparation is in high demand, and several strategies have been developed so far. Micrometer-sized GO sheets react with Fenton reagent (Fe²⁺/Fe³⁺/H₂O₂) efficiently under UV irradiation with the reaction rate strongly dependent on the extent of oxidation of the GO (Fig. 7) [39]. The photo-Fenton reaction of GO is initiated at the carbon atoms connected with hydroxyl and epoxide groups, and large amounts of hydroxyl radical and/or peroxide radical are generated under

the UV irradiation. Moreover, the newly-formed oxygen-containing groups further serve as new photo-Fenton reaction sites, and then the GO sheets with lateral size of micrometers are gradually cut into small fragments, even small molecules, and CO₂. This method provides a new strategy to prepare GQDs with peripheral carboxylic groups on a mass scale under a mild condition by simple control of the photo-Fenton reaction time.

Strong PL can be induced in single-layer graphene by employing oxygen-plasma treatment [40]. Interestingly, spatially-uniform PL is induced only in single-layer graphene on substrates and not in bi-layer or multilayer flakes. Moreover, spatially-resolved PL depends on the treatment times. In a short treatment time, emission is bright and localized, while strong, spatially homogeneous emission requires a longer treatment time.

Fig. 8 shows the first prepared uniform GQDs using self-assembled block copolymer (BCP) as an etch mask on graphene films grown by chemical-vapor deposition [41]. The results show that the GQDs are composed of monolayer or bi-layer graphene with a narrow size distribution of 10–20 nm, corresponding to the size of BCP nanospheres. Additionally, the oxygen content in the GQDs is rationally controlled by additional air-plasma treatment, which reveals the effect of the oxygen content on PL properties.

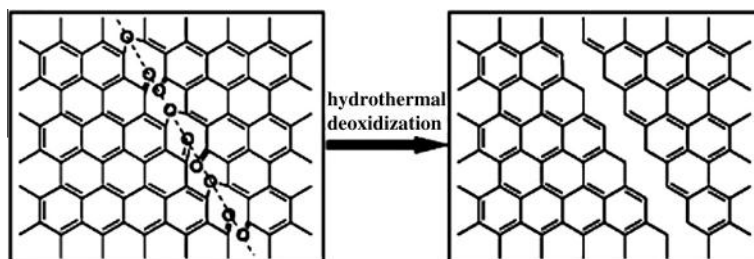


Fig. 4. Mechanism for the hydrothermal cutting of oxidized graphene sheets (GSs) into graphene quantum dots (GQDs). A mixed epoxy chain composed of epoxy and carbonyl pair groups (left) is converted into a complete cut (right) under hydrothermal treatment [15].

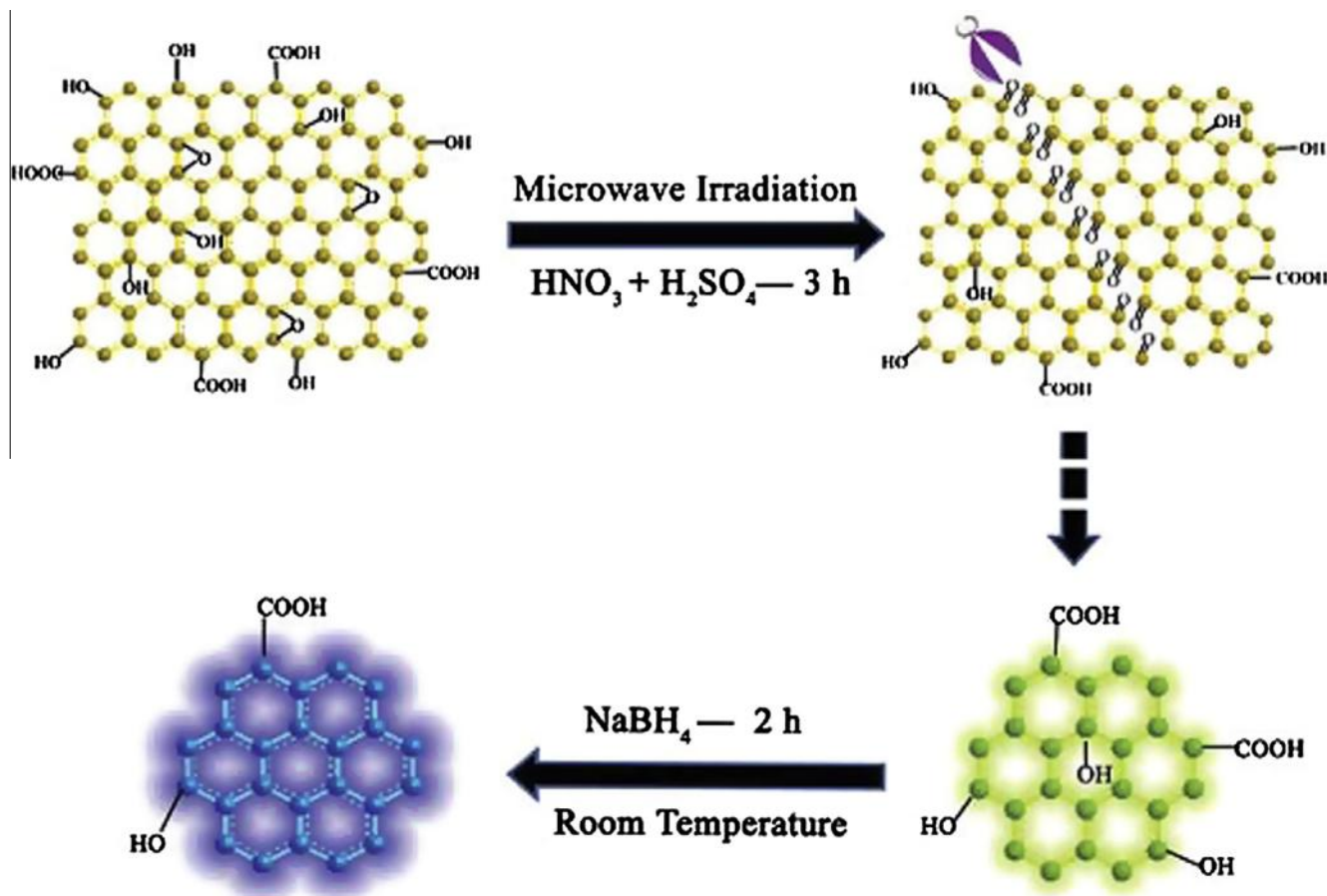


Fig. 5. The route for preparing greenish-yellow graphene quantum dots (gQDs) and blue QDs (bQDs) [37].

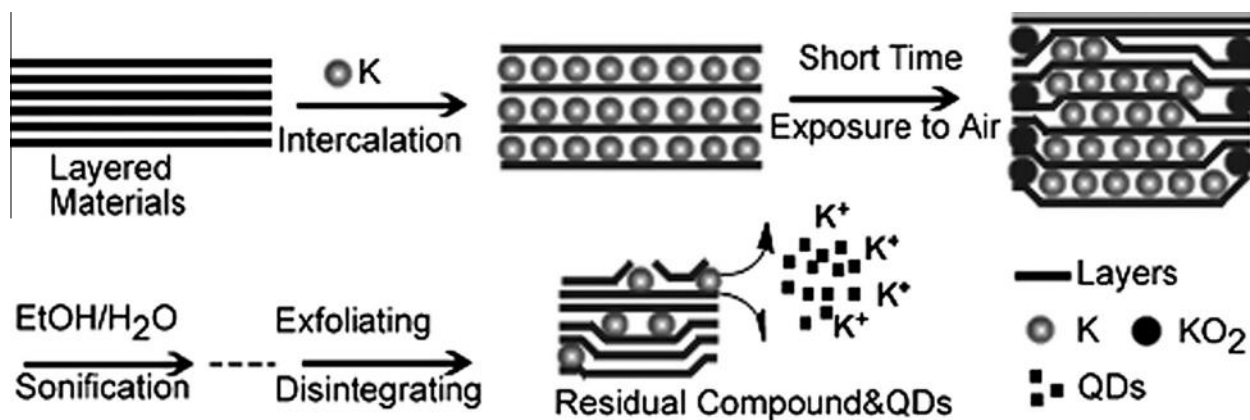


Fig. 6. The formation of graphene quantum dots (GQDs) [38].

2.1.2. Bottom-up approaches

Bottom-up approaches for the synthesis of GQDs have been carried out by many groups. An easy microwave-assisted hydrothermal method for the production GQDs derived from different sugars, including glucose, sucrose and fructose, was reported (Fig. 9) [42]. The size of the GQDs can be tuned in the range 1.65–21 nm by prolonging the heating time from 1 min to 9 min. Interestingly, most of the carbohydrates that contain C, H, and O in the ratio of ~1:2:1 are considered for use as carbon sources to prepare GQDs, since H and O exist in the forms of hydroxyl, carboxyl or carbonyl groups, which may dehydrate under hydrothermal conditions.

In 2012, luminescent GQDs and GO were selectively and successfully prepared by tuning the degree of carbonization of citric acid and dispersing the carbonized products into alkaline solutions [43]. The GQDs obtained are about 15 nm in width and 0.5–2.0 nm in thickness, while the GO consists of hundreds of nm-sized particles. GQDs obtained under moderate carbonization display strong, excitation-independent PL activity due to the abundant small sp^2 clusters contained in them; while the large-sized GO produced under high carbonization nanomaterials exhibits much lower luminescence activity, resulting from the sp^2 clusters contained in GO being isolated within the sp^3 C–O matrix.

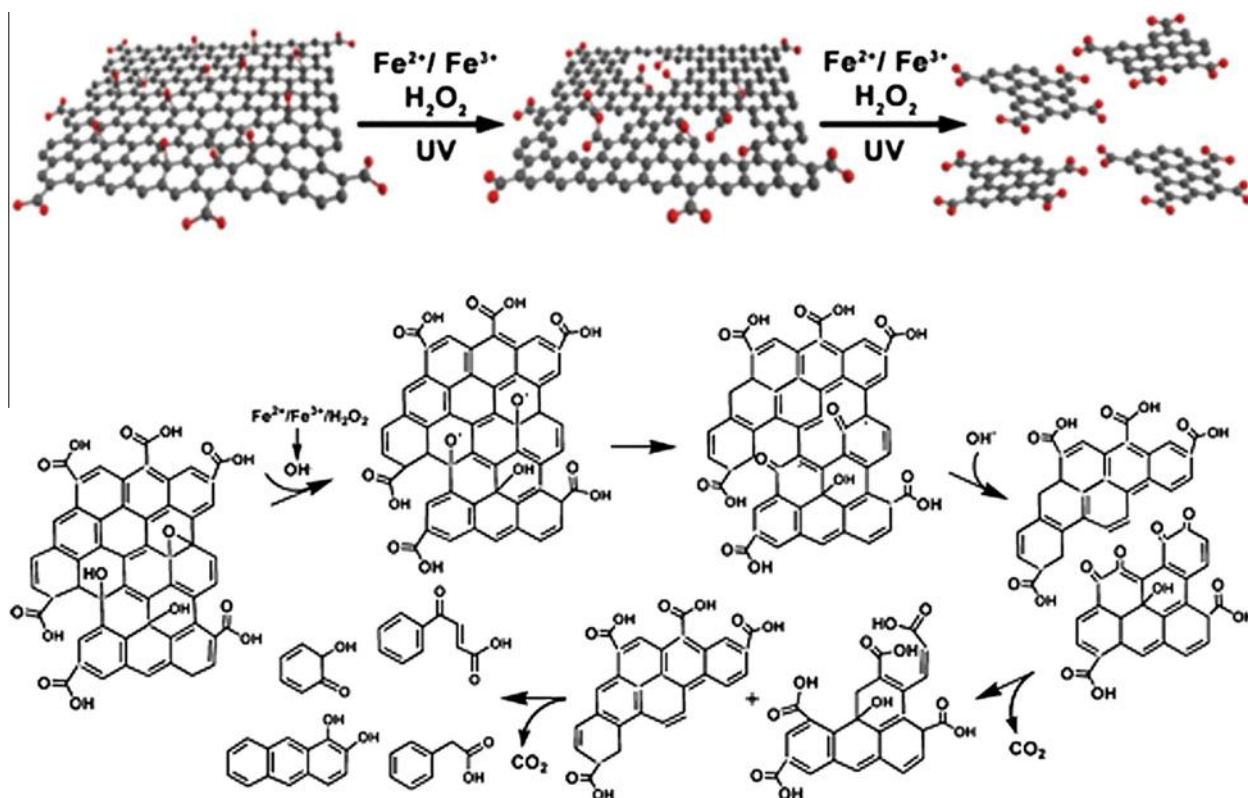


Fig. 7. A proposed mechanism for the photo-Fenton reaction of graphene-oxide (GO) sheets [39].

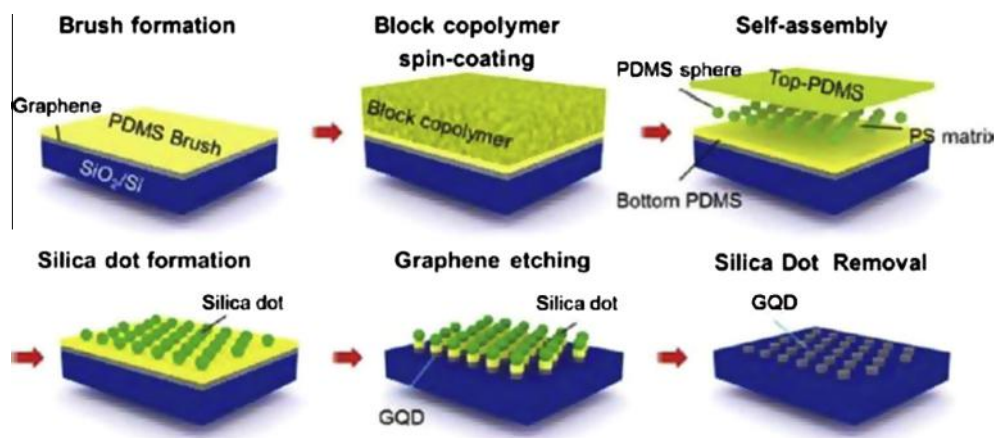


Fig. 8. The preparation of graphene quantum dots (GQDs) including the spin-coating of block copolymer (BCP), the formation of silica dots, and the etching process with oxygen plasma [41].

Multicolor photoluminescent GQDs were first prepared using unsubstituted hexa-peri-hexabenzocoronene (HBC) as a precursor in a process involving carbonization, oxidation, surface functionalization and reduction (Fig. 10) [44]. The results indicated that these mono-dispersed disk-like GQDs had a well-defined morphology and a uniform size of ~ 60 nm diameter and 2–3 nm thickness. Although the processes were complicated and time-consuming, this method provided a new way to control shape, size and composition of GQDs using different aromatic molecules.

Highly-fluorescent GQDs were prepared in 2013 via one-step pyrolysis of L-glutamic acid using a simple heating-mantle device

[45]. The selected precursors were non-toxic, common/natural materials, with nitrogen groups for easy surface modification, and free of a further capping process. The average diameter of the developed GQDs was $4.66 \text{ nm} \pm 1.24 \text{ nm}$.

Much effort has been put into the preparation of colloidal GQDs with uniform size (conjugating 168, 132 or 170 carbon atoms, respectively) and thickness via stepwise solution chemistry based on oxidative condensation reactions (Fig. 11) [46]. The twist of the substituted phenyl groups from the core plane leads to alkyl chains closing the latter in all three dimensions. As a result, stabilization of the resultant GQDs was effectively increased and the largest stable colloidal GQDs could be obtained.

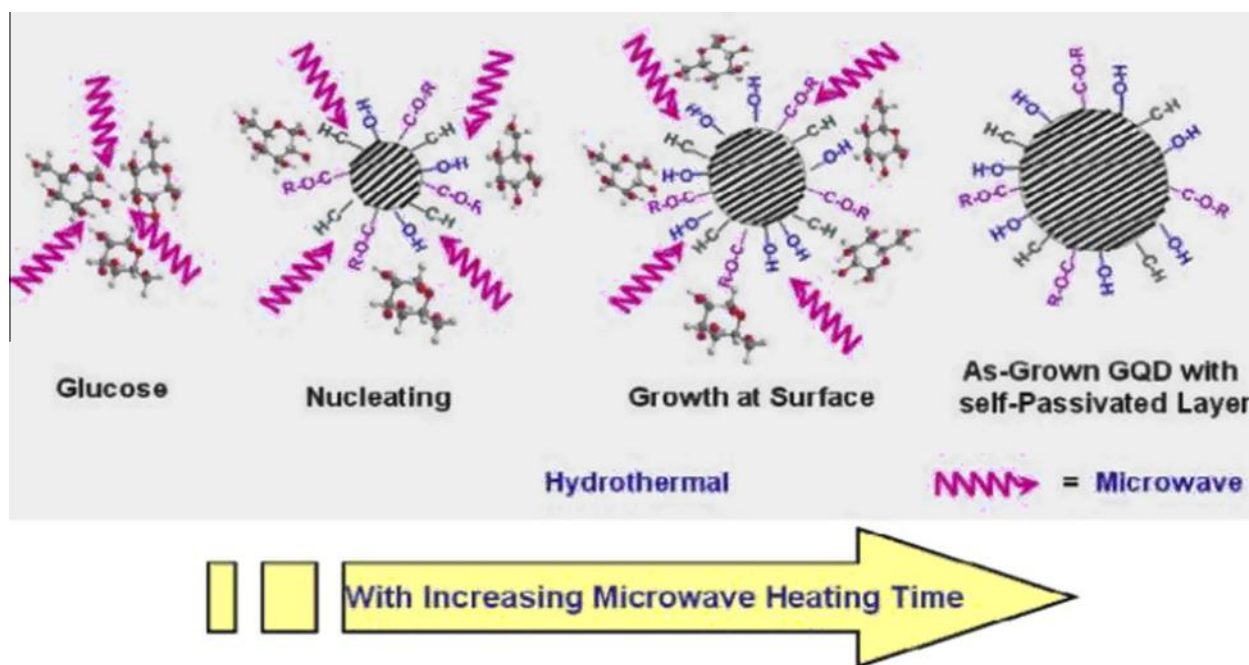


Fig. 9. The preparation of graphene quantum dots (GQDs) using the microwave-assisted hydrothermal method [42].

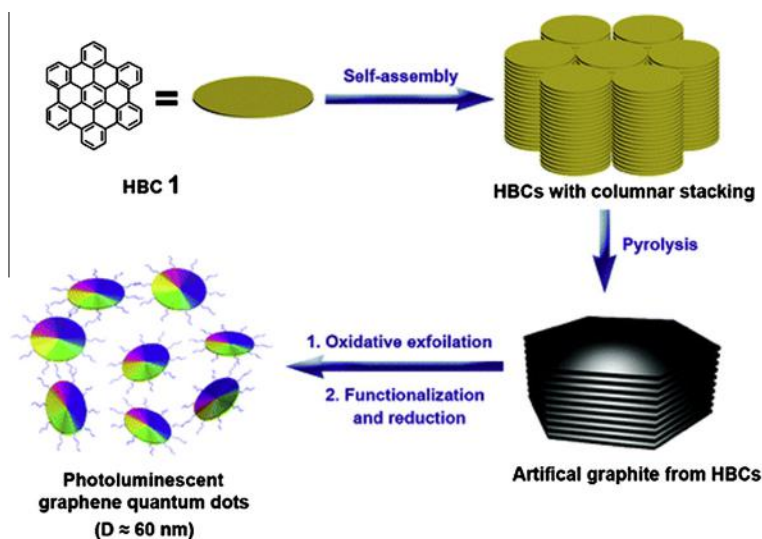


Fig. 10. Processing diagram for the preparation of photoluminescent graphene quantum dots (GQDs) by using hexa-peri-hexabenzocoronene (HBC) (1) as a carbon source [44].

2.2. Surface chemistry-tuned strategies

2.2.1. Surface functionalization

2.2.1.1. Polyethylene glycol-passivated GQDs (GQDs-PEG). GQDs-PEG were prepared by connecting the hydroxyl groups (–OH) of PEG to the carboxyl groups (–COOH) of GQDs [23]. The prepared GQDs-PEG showed strong blue PL under 365 nm with a quantum yield of about 28.0%. The upconversion PL images could be observed under a fluorescence microscope coupled with an 808 nm laser. Furthermore, the GQDs-PEG appeared to have higher photon-to-electron conversion capability compared with GQDs from photoelectrode construction.

Greater fluorescence performance and upconversion properties of surface-passivated GQDs with oligomeric PEG diamine (PEG1500N) were also reported [22]. First, GO was further oxidized

by HNO_3 , and cut into small GO sheets. Then, the precursor was treated with the surface-passivation agent and finally reduced by hydrazine hydration to fabricate GQDs (Fig. 12). These GQDs showed strong blue emission and green fluorescence under the excitation at 365 nm or using a 980 nm laser. Interestingly, the fluorescence results of GQDs resembled those of band-gap transitions, while the upconverted PL properties of GQDs were similar to the anti-Stokes PL, and there was a constant energy difference between the excitation and emission light.

2.2.1.2. Amine-functionalized GQDs. The amine-functionalized method is commonly applied to modify graphene-based materials, which effectively decreases the surface defects for fluorescence enhancement. A novel graphene nanostructure edge-terminated by a primary amine starting from oxidized graphene sheets (OGSs)

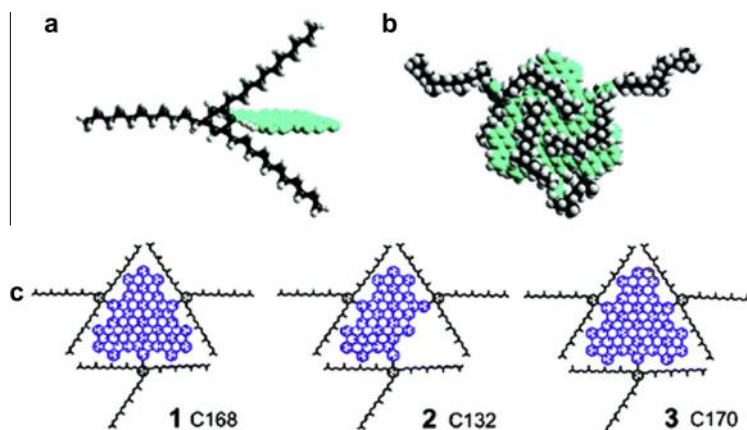


Fig. 11. The preparation of colloidal size-uniform graphene quantum dots (GQDs) with stepwise solution chemistry. (a) A 2',4',6'-trialkyl-substituted phenyl moiety is covalently attached to the edges of the graphene to force the peripheral phenyl groups to twist from the plane of the graphene; (b) an energy-minimized geometry of the GQD 1 (in c), showing the "caging" of the graphene core (blue) by the alkyl chains (black) in three dimensions; and, (c) structures of the three largest colloidal GQDs synthesized so far, containing 168, 132, or 170 conjugated carbon atoms, respectively [46].

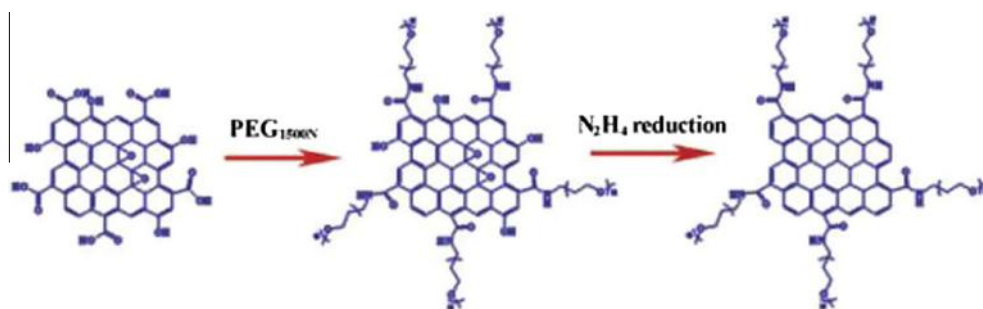


Fig. 12. Graphene quantum dots (GQDs) containing an oligomeric polyethylene glycol (PEG) diamino surface passivating agent [22].

has been designed [20]. The OGSs were subjected to mild amino-hydrothermal treatment at 70–150°C using ammonia solution, followed by thermal annealing at 100°C (Fig. 13a). In the treatment of OGSs, ammonia reacted with epoxy groups to form a primary amine and alcohols through nucleophilic substitution, which enabled self-limited extraction of the sp^2 domains by ring-opening of the epoxide and the simultaneous direct bonding of a primary amine with a graphene edge. Consequently, size-controlled GQDs edge-terminated with a primary amine were produced.

In another study, the fabricated GQDs were functionalized with amine groups using the sequential oxidation and reduction of GO. The GQDs obtained were 1–3 layers in thickness and less than 5 nm in diameter [24]. These functionalized GQDs exhibited a red-shift of PL emission (~ 30 nm) compared to the unfunctionalized GQDs, which was attributed to charge transfers between functional groups and GQDs. Furthermore, the photoluminescent emissions of both GQDs and amine-functionalized GQDs were also shifted with the pH change, due to protonation or deprotonation of the functional groups. This study was the first to tune and to identify the change of the band gap in GQDs through the charge distribution between the GQDs and the functional groups.

Size-controlled, amine-functionalized GQDs with diameters of 7.5 nm were prepared from GO sheets, ammonia and hydrogen peroxide as starting materials [47]. In the procedure, hydrogen peroxide and ammonia played a synergistic role on GO sheets, where the hydrogen peroxide cut GO sheets into smaller sizes and the ammonia passivated the active surface to give amine-modified GQDs (Fig. 13b). These GQDs exhibited multicolor fluorescence at 420 nm.

The surface chemistry of GQDs was programmably tuned through modification or reduction and their emission changed from green to blue [48]. The experimental results demonstrated that the $-COOH$ and epoxy of GQDs changed into $-CONHR$ and $-CNHR$ in these modified GQDs (m-GQDs) during modification and the carbonyl, epoxy and amido moieties into $-OH$ groups in reduced GQDs (r-GQDs) during reduction. As a result, the non-radiative recombination of localized electron-hole pairs decreased and the integrity of surface π electron network was enhanced, which proved that the intrinsic state emission played a key role in the preparation of GQDs. The results of time-resolved measurements were also consistent with the suggested PL mechanism.

2.2.1.3. Aryl-modified GQDs. Diazonium chemistry is an effective method for functionalizing graphene materials. Chemically-modified GQDs were reported with different aryl groups, including phenyl, 4-carboxyphenyl, 4-sulfonylphenyl and 5-sulfonaphthyl, via the Gomberg–Bachmann reaction (Fig. 14) [21]. The aryl-modified GQDs were nanocrystals with lateral dimensions in the range 2–4 nm, and average thickness <1 nm. The modification of aryl groups did not only change the edge structures of the GQDs and protect their PL active edging sites, but also introduced the interaction of graphene basal planes and aryl grafts. Thus, because of the resonance effects between aryl groups and graphene basal planes, the PL bands of GQDs were systematically tuned with their fluorescence quantum yield and pH tolerance greatly improved. This result indicated that diazonium chemistry was a convenient, effective technique for chemical modification of GQDs, and also shone a light on the mechanism of their PL emission.

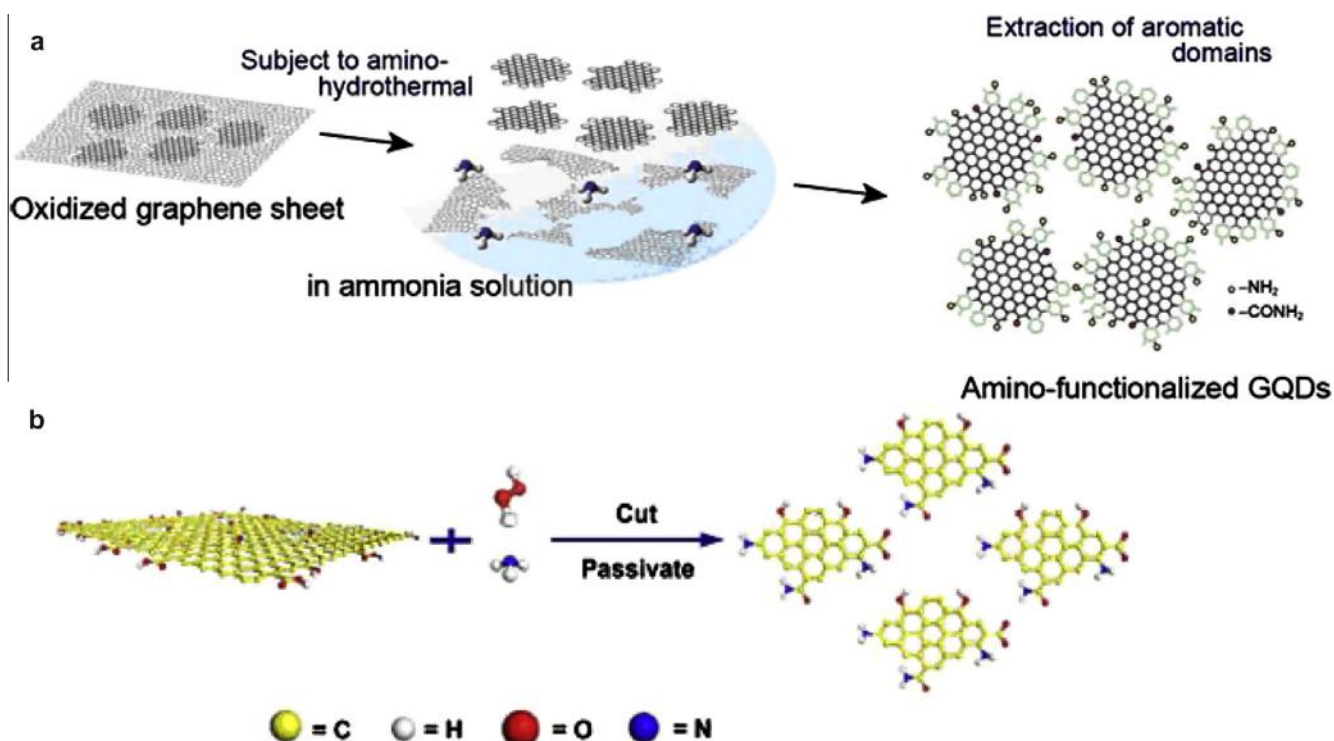


Fig. 13. (a) The strategy for preparing amino-functionalized graphene quantum dots (GQDs) [20], and (b) size-controlled amine-functionalized GQDs [47].

2.2.2. Doping with other elements

2.2.2.1. N-doped GQDs. Nitrogen doping is a powerful way to modify the properties of carbon materials ranging from activated carbon to graphene [49–51]. Accordingly, nitrogen-doped GQDs (N-GQDs) have also been prepared and the results showed that N-GQDs with chemically-bonded N atoms can dramatically alter their electronic characteristics and offer more active sites, thus presenting new phenomena and unexpected properties. A simple electrochemical approach to luminescent and electrocatalytically-active N-GQDs with oxygen-rich functional groups was reported [25]. Compared with their green-luminescent N-free counterparts of similar size (2–5 nm), the newly produced N-GQDs with an N/C atomic ratio of $\sim 4.3\%$ emitted blue luminescence. Highly blue-luminescent N-GQDs with a quantum yield of 24.6% were obtained using hydrothermal treatment of GO in the presence of ammonia at 180°C [26] without strong acid treatment or further surface modification (Fig. 15).

N-doped graphene was first synthesized by annealing reduced GO in a tube furnace at 300°C for 1 h in an ammonia atmosphere [27]. Then, the N-GQDs with a diameter of $\sim 1\text{--}7\text{ nm}$ and an N/C atomic ratio of $\sim 5.6\%$ were obtained by cutting N-doped graphene via a simple hydrothermal approach. The N-GQDs exhibited bright fluorescence performance and excellent upconversion properties. The solution chemistry approach was applied to the synthesis of N-GQDs [52]. In addition to two N atoms, the conjugated cores of QDs 1 and 2 contained 176 and 128 carbon atoms. The numbers of N atoms in the QDs were controlled and their bonding configurations defined so that 1 and 2 could be made in the aryl-annulated phenazine style. This method produced N-GQDs with well-defined properties in contrast to the previous methods explored for N-GQDs. This method is applicable to the synthesis of GQDs doped with N atoms in other bonding configurations.



Fig. 14. The scheme for modifying graphene quantum dots (GQDs) with aryl groups via the Gomberg–Bachmann reaction [21].

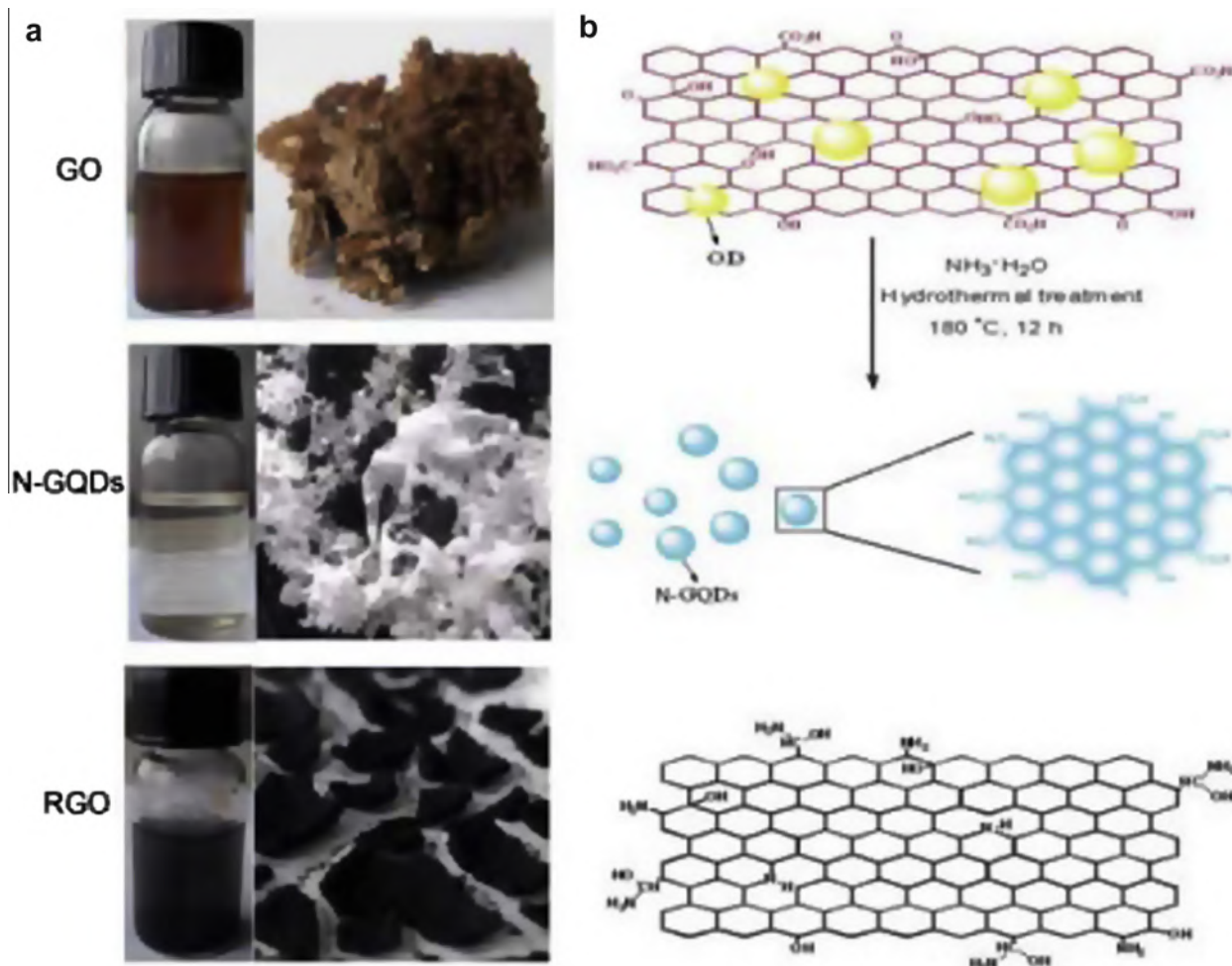


Fig. 15. (a) Typical pictures of water dispersions and solid samples of graphene oxide (GO), nitrogen-doped QDs (N-QDs) and reduced GO (RGO); (b) the preparation of N-QDs with hydrothermal treatment of GO in the presence of ammonia [26].

2.2.2.2. F-doped QDs (F-QDs). Graphene doped with fluorine can effectively engineer a tunable gap in the energy spectrum of graphene and thus produce new phenomena and properties due to the high electronegativity of the fluorine atom [53,54]. Consequently, F-QDs were prepared with an F/C atomic ratio of ~23.68% and a diameter of 1–7 nm by cutting fluorinated graphene via the hydrothermal approach [28]. The F-QDs displayed bright blue and a clear upconversion PL, which may expand the applications of fluorinated graphene in environmental and energy technology. Moreover, compared to QDs, the maximum PL peak of F-QDs showed a red-shift by ~10 nm in the PL emission spectra, which may be due to the relatively high surface-defect concentration in the F-QDs resulting from the high degree of fluorination.

3. Physical and chemical properties

3.1. Optical properties

3.1.1. Absorbance and PL

The absorption-peak position of QDs depends on the preparation method and their size for a quantum-confinement effect. QDs exhibited a characteristic absorption around 230 nm, attributed to π - π^* transition of C=C within the graphene structure, with a tail extending out into the visible range [15,32,36,38,45]. Some of

the QDs obtained had an absorption peak around a wavelength in the range 270–360 nm due to the $n \rightarrow \pi^*$ transition of C=O [23,26,30,35,37,44,55,56]. For example, the large disk-like QDs of around 60 nm in size exhibited a weak absorption shoulder at 280 nm [44], which approximated to that of N-doped QDs (size 2–3 nm) obtained via the electrochemical approach with an absorption band at ~270 nm [25]. In addition, the preparation method and their size were also associated with the PL characteristics of QDs, and, so far, the resultant QDs emitting PL have been prepared with different colors ranging from deep ultraviolet [42] to blue [15,23,24,33,37,43,57], green [35], greenish-yellow [37], yellow [55] and red [31] under 365 nm UV light.

Although the exact mechanism of PL is still an enigma, theories proposed for the PL phenomenon include electron-hole recombination, quantum-size effect/free zig-zag sites with a carbene-like triplet ground state, doping, edge structure, and surface defects in the functional groups of the QDs. In general, most luminescent QDs exhibit excitation-dependent PL characteristics with an emission-peak shift towards longer wavelength accompanied with an intensity decrease when the excitation wavelength is a bathochromic shift.

However, there were also a few exceptions. As shown in Fig. 16a, QDs derived from citric acid showed an excitation-independent PL feature [43]. When the excitation wavelength changed from 300 nm to 440 nm, the maximum emission wavelength still remained at 362 nm while the intensity decreased. This

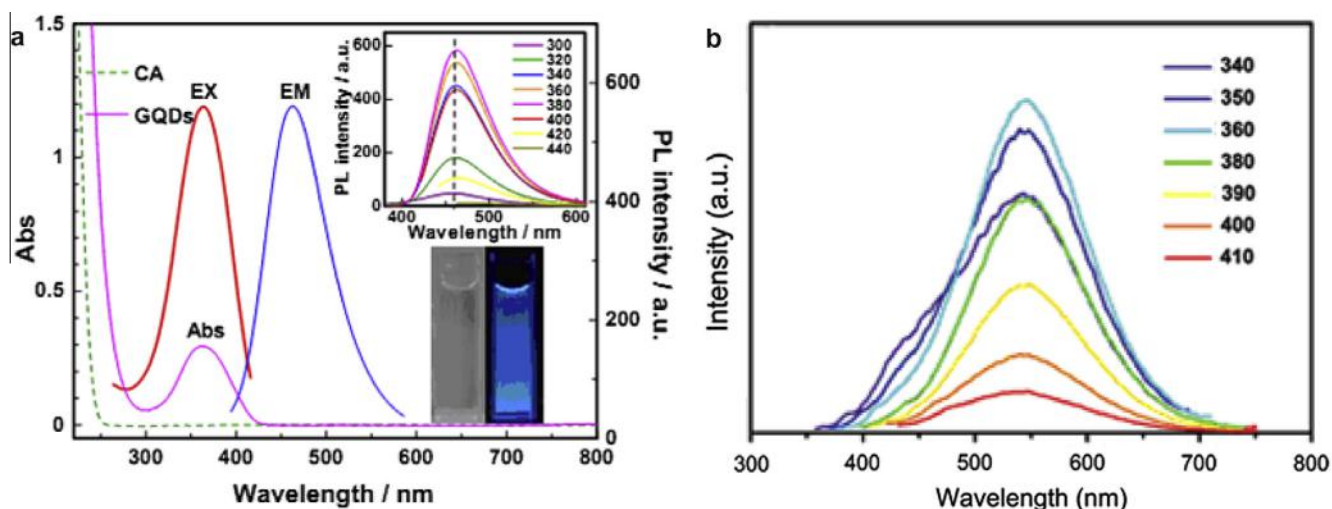


Fig. 16. (a) UV-Vis absorption of citric acid (CA) and the graphene quantum dots (GQDs), and the photoluminescence (PL) spectra of the GQDs. Insets: (Upper) Emission spectra of the GQDs with excitation at different wavelengths; (Lower) Photographs of GQD solution taken under visible light (left) and under 365 nm UV light (right) [43]; (b) PL spectra of the GQD aqueous solution at different excitation wavelengths [55].

phenomenon was attributed to both the uniform size and the surface state of those sp^2 clusters contained in GQDs. Another report noted that the intensity of PL increased to the maximum value and then decreased, but that the fluorescent emission peak remained unshifted when the excitation wavelength shifted from 340 nm to 410 nm (Fig. 16b) [55].

The PL spectra of GQDs exhibited pH-dependent characteristics. For example, the central peak wavelengths of the PL spectra of the GQDs generated by the photo-Fenton reaction were invariant in the range pH 3–10, but the PL intensity of the GQDs was much stronger in pH 10 than in pH 3. As electron donors, the negatively-charged carboxylate groups in the GQDs may have taken a key role in the PL procedure (Fig. 17a) [39]. Under alkaline conditions, the GQDs emitted strong PL but the PL was obviously quenched under an acidic conditions. If the solution pH was switched repeatedly between 13 and 1, the PL intensity varied reversibly (Fig. 17b) [15]. This reversible phenomenon can be understood well, based on the proposed structural models (Fig. 17c). Under the acidic conditions, the free zig-zag sites of the GQDs were protonated, forming a reversible complex between the zig-zag sites and H^+ . Thus, the emissive triple carbene state was broken and became inactive in PL. However, under the alkaline conditions, the free zig-zag sites were restored, thereby leading to the restoration of PL. A similar phenomenon and scheme were also proposed [58].

Partial GQDs are sensitive to the species of solvent. The emission wavelength of GQDs obtained using the one-step solvothermal method shifted from 475 nm to 515 nm in tetrahydrofuran (THF), acetone, dimethylformamide (DMF), and water. This could

be induced by solvent attachment or different emissive traps on the surface of GQDs (Fig. 18a) [35]. However, a blue shift of the GQDs could be observed in the solvent change from water, DMF, or acetone to THF, while m-GQDs and r-GQDs exhibited negligible solvent-dependent behaviors (Fig. 18b), which were associated with the emissive traps on the surface of the GQDs induced by solvent attachment [48].

3.1.2. Upconverted PL

In addition to the strong PL, the upconverted PL feature of GQDs was reported. Fig. 19a shows the PL spectra of GQDs excited by long-wavelength light at ~ 407 nm for the upconverted emissions. Remarkably, the upconversion PL also shows an excitation-independent behavior with the red shift in the excitation wavelength. The authors attributed this upconverted PL property to the multi-photon active process [59], the same mechanism reported elsewhere [56]. However, there are still different views concerning the explanation for this phenomenon. One view is that an upconverted PL can be observed when the π electrons are excited from the σ orbital transition back to the σ orbital, while the electrons of the σ orbital transition to the σ orbital result only in normal PL (Fig. 19b) [22].

3.2. Cytotoxicity

GQDs are very stable and are free of heavy metal ions, thus revealing promise for applications in various biological fields. So far, the inherent toxicities of GQDs have been evaluated by the cell-viability assay {e.g., Hela cells [47], MC3T3 cells [48], and

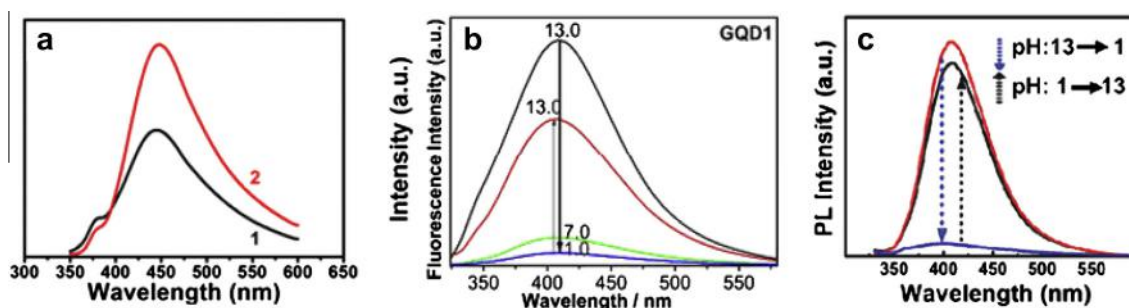


Fig. 17. (a) Photoluminescence (PL) spectra of graphene quantum dots (GQDs) suspended in the water with pH values of 3 (line 1) and 10 (line 2) [39]; (b) Fluorescence spectra of GQD1 (a) in water solution when the pH is shifted between 1.0 and 13.0; (c) pH-dependent PL spectra when the pH is switched between 13 and 1 [15].

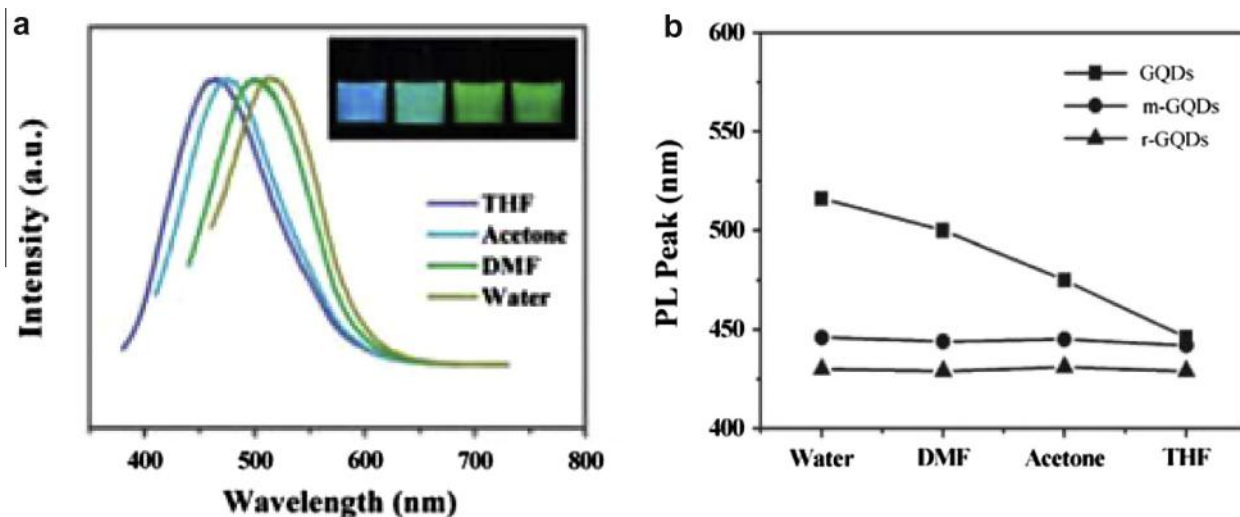


Fig. 18. (a) Effect of solvents on the fluorescence of graphene quantum dots (GQDs) (at 375 nm excitation). Inset: photograph of the four dispersions taken under UV light [35]; (b) Solvent-dependent photoluminescence (PL) of GQDs, modified GQDs (m-GQDs) and reduced GQDs (r-GQDs). PL peaks are collected at 380 nm excitation for GQDs and 360 nm excitation for m-GQDs and r-GQDs [48].

A549 cells [57]. The results indicated that GQDs possess excellent biocompatibility and low cytotoxicity. As shown in Fig. 20a, GQDs show negligible cytotoxicity at concentrations $<0.5 \text{ mg mL}^{-1}$, indicating excellent biocompatibility [47]. GQDs and r-GQDs appeared to have very low toxicity to MC3T3 cells, with relative cell viability higher than 80% up to the addition of 400 μg , while over 40% cells were inhibited when 400 μg of m-GQDs were added (Fig. 20b) [48]. It is speculated that this difference was attributable to the connected methylamine, in which both nitrogen and alkyl chains affected the circumstances of the cells.

3.3. Electrocatalytic activity

N-CNTs [60] and N-graphene [61,62] can act as metal-free electrocatalysts to replace the commercially-available platinum (Pt)-based catalysts for the oxygen-reduction reaction (ORR). N-GQD/graphene film after hydrothermal treatment could exhibit good conductivity of $\sim 40 \text{ S cm}^{-1}$ and superior electrocatalytic ability for the ORR [25]. A well-defined cathodic peak clearly occurred

in the O_2 -saturated but not the N_2 -saturated KOH solution for N-GQDs/graphene (Fig. 21a), and the ORR onset potential at $\sim -0.16 \text{ V}$ with a reduction peak at $\sim -0.27 \text{ V}$ indicated significant catalytic ability of N-GQD/graphene for the ORR (Fig. 21b). The control result that N free-GQDs/graphene had no obvious ORR electrocatalytic activity suggested the critical role of N-doping. Moreover, the current density relied on the rotation rate due to the diffusion of electrolytes (Fig. 21c). More importantly, there was no obvious decrease in current observed after two days of continuous cycling in O_2 -saturated 0.1 M KOH, indicating the catalytic activity of the N-GQD/graphene electrode was stable (Fig. 21d). Similar electrocatalytic ability was observed in colloidal N-GQDs [52,63]. Moreover, the electrocatalytic activity for the ORR of colloidal N-GQDs was size-dependent.

3.4. Electrochemiluminescence

The gQDs and the bQDs obtained showed electrochemiluminescence (ECL) behavior with a maximum wavelength at 512 nm

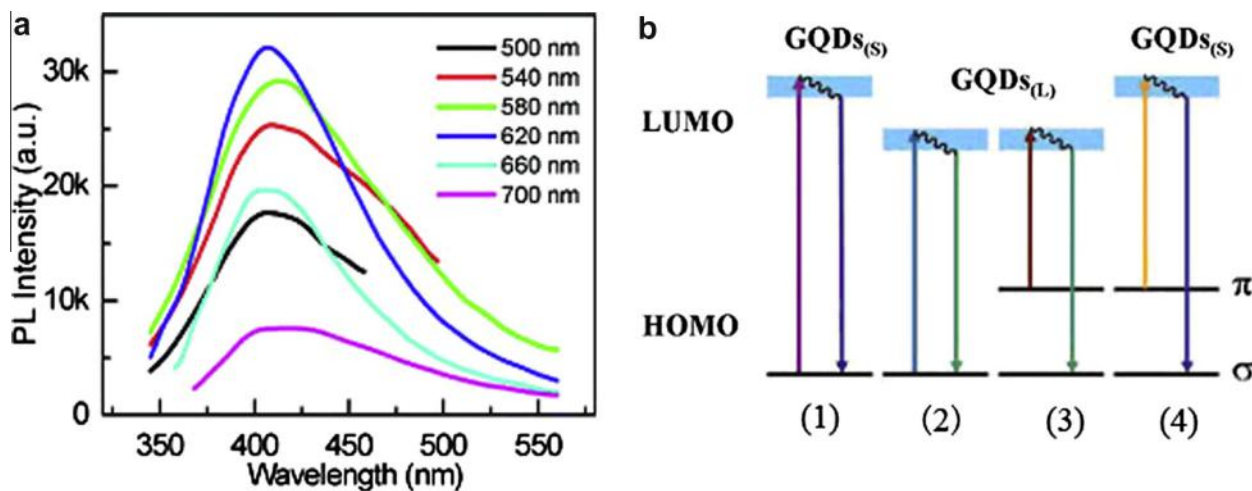


Fig. 19. (a) Upconverted photoluminescence (PL) spectra of the graphene quantum dots (GQDs) at different excitation wavelengths [59]. (b) Various typical electronic transition processes of GQDs. Normal PL mechanisms in GQDs for small size (1) and large size (2). Upconverted PL mechanisms in GQDs for large size (3) and small size (4) [22].

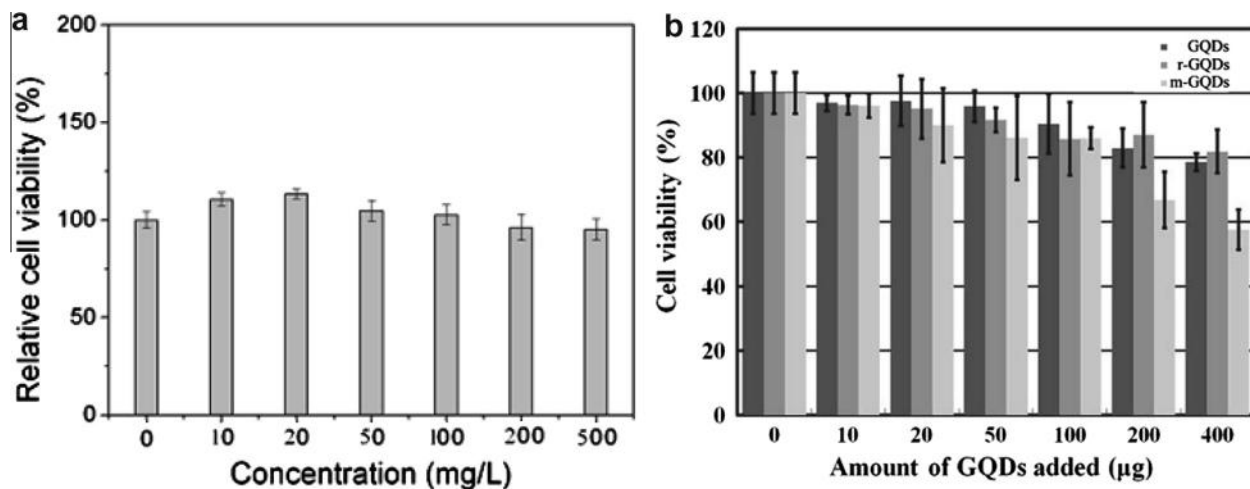


Fig. 20. (a) Cellular viability of HeLa cells (normalized to the untreated control) incubated with graphene quantum dots (GQDs) (0–500 mg L⁻¹) for 24 h. The data in each column were obtained from three repeats and statistically analyzed using Student's t-test [47]; (b) Effect of GQDs, modified GQDs (m-GQDs) and reduced GQDs (r-GQDs) on MC3T3 cell viability [48].

in 0.05 M, Tris-HCl buffer solution (pH 7.4) with 0.1 M K₂S₂O₈ as coreactant. As seen in Fig. 22a, gGQDs showed an intense ECL emission at -1.45 V, with an onset potential at about -0.9 V. Moreover, apart from the reduction peak of S₂O₈²⁻ around -0.8 V in the CVs of

the background and gGQDs, a small peak appears at -1.36 V assigned to the reduction peak of the gGQDs that appeared. The relatively positive potential of gGQDs indicated that the high content of sp² carbon domains in the gGQDs inherited from graphene

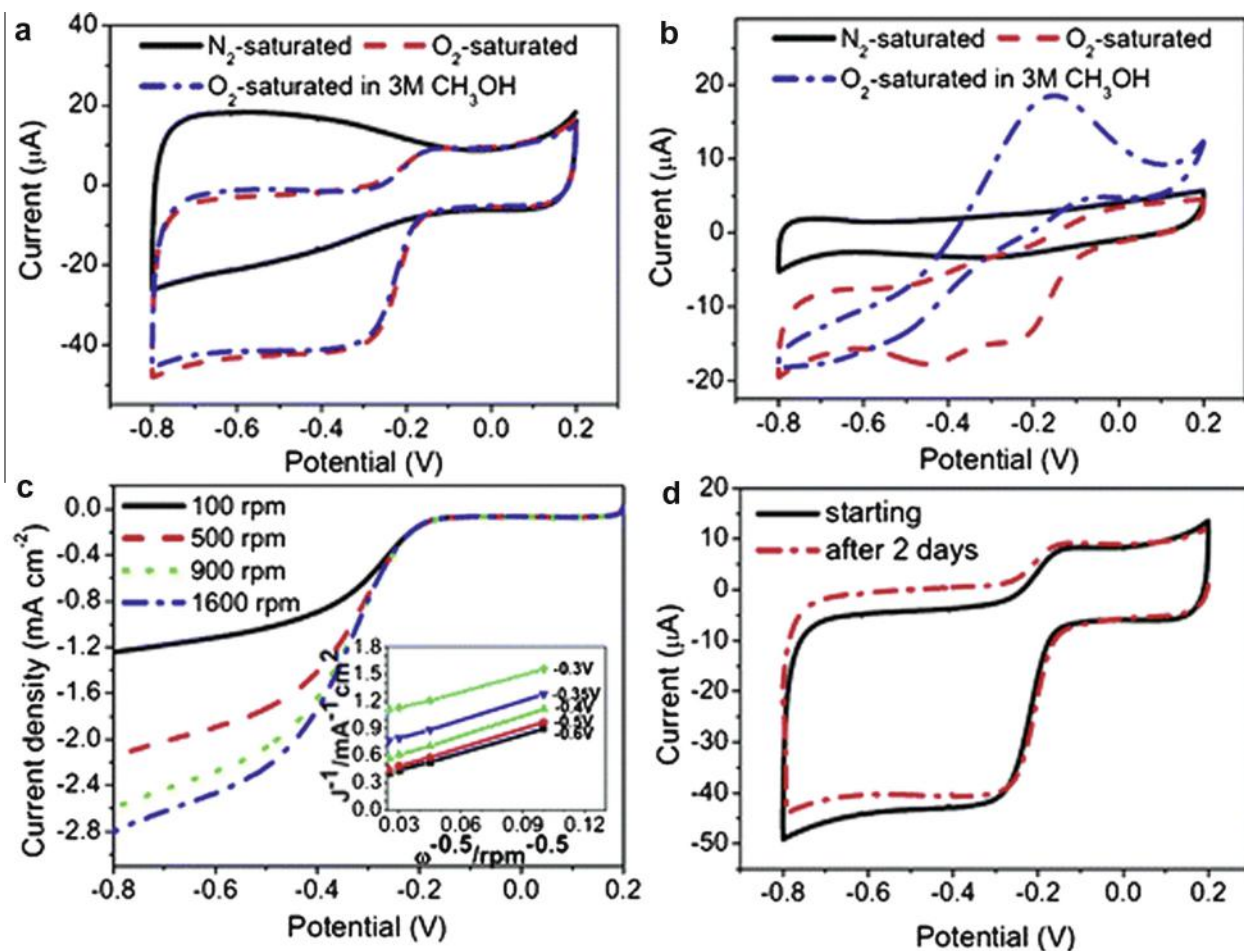


Fig. 21. Cyclic voltammograms (CVs) of (a) nitrogen-doped GQDs (N-GQDs)/graphene and (b) commercial Pt/C on a glassy-carbon (GC) electrode in N₂-saturated 0.1 M KOH, O₂-saturated 0.1 M KOH, and O₂-saturated 3 M CH₃OH solutions; (c) Rotating disk electrode (RDE) curves for N-GQDs/graphene in O₂-saturated 0.1 M KOH at different speeds. The inset shows the Koutecky–Levich plots derived from the RDE measurements; (d) Electrochemical stability of N-GQDs/graphene, as determined using continuous cyclic voltammetry in O₂-saturated 0.1 M KOH [25].

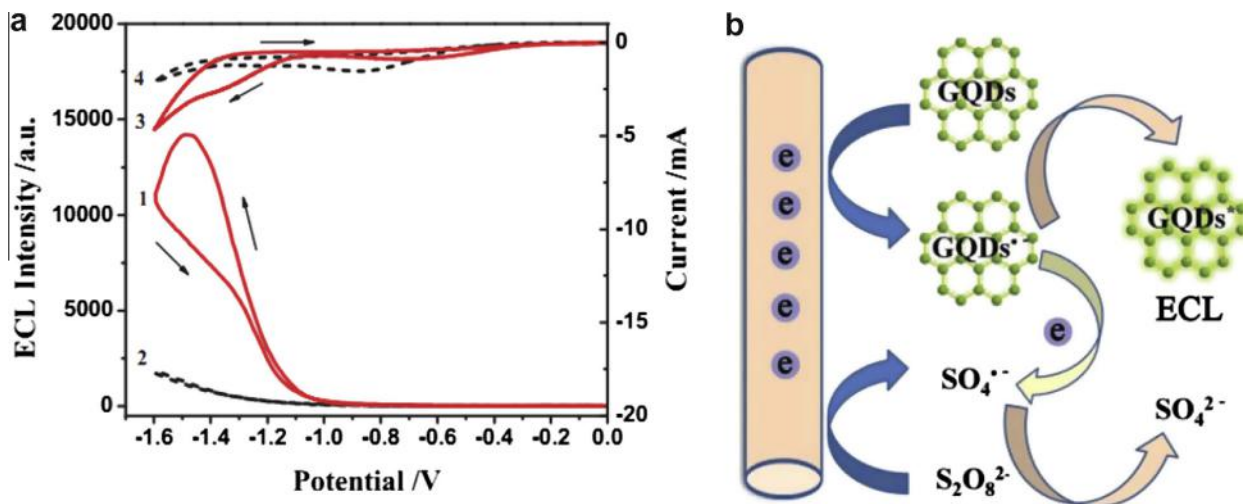


Fig. 22. (a) Electrochemiluminescence (ECL)-potential curves and CVs of the greenish-yellow GQDs (gGQDs) (1,3) and background (2,4) with a concentration of 20 ppm in 0.05 M Tris-HCl (pH 7.4) buffer solution containing 0.1 M K₂S₂O₈. Scan rate: 100 mV s⁻¹; (b) ECL mechanism of GQDs [37].

could accelerate electron transport during the ECL process. However, the ECL intensity of bGQDs was weaker than that using gGQDs due to the higher band gap and the greater reduction resistance than those of gGQDs. The possible ECL mechanism revealed that the strong oxidation radicals, SO₄^{•-} and GQDs^{•-}, produced in the electrochemical reduction of S₂O₈²⁻ and GQDs, then reacted with each other to generate an excited state product (GQDs*) via electron-transfer annihilation, resulting in light emission [37].

4. Applications

4.1. Environmental

Recently, various optical sensors were constructed based on signal-off or signal-on processes because of the excellent luminescent properties of GQDs. A fluorescence-sensing platform based on GQDs was designed for ultrasensitive detection of 2,4,6-trinitrotoluene (TNT) using fluorescence resonance-energy transfer (FRET) quenching via the π - π stacking interaction between GQDs and the aromatic rings of TNT [64]. TNT bound on surface of the GQDs strongly suppressed the fluorescence emission from the donor GQDs to the irradiative TNT acceptor at spatial proximity. The attenuation of fluorescence intensity could clearly be detected

down to 0.495 ppm (2.2 mM) in the linear range 4.95×10^{-4} – 1.82×10^{-1} g L⁻¹ of TNT.

Free chlorine could significantly quench the fluorescence signal of GQDs by destroying their passivated surface (Fig. 23) [65]. Under optimal experimental conditions, the limit of detection (LOD) of free chlorine was 0.05 μ M in the range 0.05–10 μ M. Moreover, the sensing system was applied to the detection of free residual chlorine in tap-water samples, and the results agreed well with those obtained using the *N*-*N*-diethyl-*p*-phenylenediamine colorimetric method. These results suggested potential application of this sensing system to monitoring of drinking water quality.

Since the Eu³⁺ ion displayed higher affinity for the oxygen-donor atoms in phosphate (Pi) than the carboxylate groups on the surface of GQDs, a specific PL off-on assay was designed for the detection of Pi [66]. Initially, GQD aggregation could be induced by the presence of Eu³⁺, which quenched the PL of GQDs through energy-transfer or electron-transfer processes. Then, GQD aggregation was dissociated due to the introduction of Pi. The sensing assay showed a rapid response within 5 min with an LOD of 0.1 μ M in the concentration range of 0.5–190 μ M Pi.

Similarly, a fluorescence “off-to-on” mechanism of GQDs@GSH was proposed for the assay of ATP, since the fluorescence of GQDs@GSH was eventually switched off with increasing concentration of Fe³⁺ caused by the effective electron transfer from the

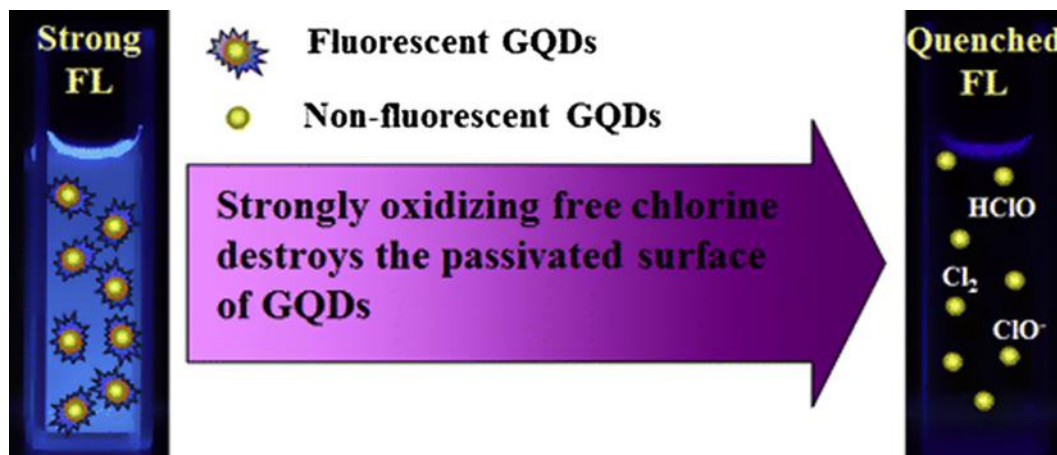


Fig. 23. Free chlorine destroying the passivated surface of graphene quantum dots (GQDs) [65].

GSH on the surface of the GQDs@GSH to Fe^{3+} [67]. The quenched fluorescence of the GQDs@GSH basically recovered in the presence of phosphate-containing molecules because of the high affinity for Fe^{3+} through the Fe–O–P bonds. This sensitive assay has been applied to estimate the concentration of ATP in cell lysates and human-blood serum, and the results agreed with the normal level of ATP of 2–10 mM in cells. Furthermore, taking into account the special coordinate interaction between Fe^{3+} and phenolic hydroxyl, a sensitive, selective probe for Fe^{3+} detection with an LOD of 1 ppm based on the fluorescence quenching of GO nanosheets was designed. The fluorescence quenching resulted from the reaction between the alpha-hydroxy quinoid six-membered ring and Fe^{3+} [68]. In addition, six ions (Ni^{2+} , Pb^{2+} , Cu^{2+} , Co^{2+} , Fe^{2+} and Cd^{2+}) could quench the ECL of gGQDs in the Tris-HCl buffer solution (0.05 M, pH 7.4) containing 0.1 M $\text{K}_2\text{S}_2\text{O}_8$ and 20 ppm gGQDs [37]. In particular, 20 μM Cd^{2+} could cause a 92% ECL intensity decrease in gGQDs as a result of the coordination reaction between Cd^{2+} and the coordination groups on the surface of the gGQDs.

Furthermore, GQDs showed high peroxidase-like activity. GQDs were assembled on an Au electrode using cysteamine as a cross-linker [69]. The resultant covalently-assembled GQD/Au electrode with good stability and reusability performed well in H_2O_2 detection. The GQD/Au electrode displayed a rapid amperometric response to H_2O_2 in 10 s with a low LOD down to 0.7 μM in the range 0.002–8 mM. On account of its good electrocatalytic activity and high stability, the GQD/Au electrode was applied to detect H_2O_2 in physiology and pathology.

4.2. Bioanalytical

4.2.1. Detection of biological molecules

The low toxicity, excellent solubility, and biocompatibility of GQDs have facilitated their promising application in biological sensors. A novel glucose-sensing system was designed based on combining affinity sensing and electrostatic attraction between anionic fluorescent GQDs and a cationic boronic acid-substituted bipyridinium salt (BBV) [70]. Fig. 24 shows that the electrostatic attraction between GQDs and BBV resulted in the excited-state

electron transfer from the GQDs to bipyridinium and quenched the fluorescence intensity of the GQDs. The tetrahedral anionic glucoboronate esters formed in the presence of glucose effectively neutralized the net charge of the cationic bipyridinium, and recovered the fluorescence intensity of the GQDs. The sensor needed no further chemical modification of the GQDs and offered a convenient “mix-and-detect” protocol for homogeneous, rapid detection of glucose within 5 min.

A glucose biosensor using GQDs as enzyme-immobilization substrate-modified carbon ceramic electrode (CCE) was also developed [71]. When the glucose oxidase was immobilized, the biosensor responded efficiently to glucose in the range 5–1270 mM with an LOD of 1.73 mM, and a sensitivity of 0.085 $\text{mA mM}^{-1} \text{cm}^{-2}$. The high performance of the biosensor was attributable to the large surface-to-volume ratio, excellent biocompatibility of the GQDs, porosity of the GQD/CCE, and the abundance of the hydrophilic edges and the hydrophobic plane in the GQDs. These studies confirmed the outstanding performance of GQDs in electrochemical biosensors.

A luminescence resonance-energy transfer (LRET) immunosensor used graphene as acceptor and mouse anti-human immunoglobulin G (mIgG, antibody) conjugated-GQDs as donor for detecting human immunoglobulin G (IgG, antigen) (Fig. 25) [72]. With the addition of graphene to the mIgG-GQDs solution, both the π – π stacking interaction between graphene and GQDs, and the non-specific binding interaction between mIgG and the graphene surface brought graphene and GQDs into LRET proximity to facilitate luminescence quenching of the GQDs. The luminescence was restored because the specific antibody–antigen interaction occurring between human IgG and mIgG increased the distance between the mIgG-GQDs and the graphene surface and thus hindered the LRET process. Under optimal conditions, this signal-on immunosensor presented good sensitivity and selectivity with an LOD of 10 ng mL^{-1} in the range 0.2–12 $\mu\text{g mL}^{-1}$.

Also, taking advantage of the fluorescence quenching of GQDs, a turn-off sensor for Ag^+ and biothiol detection was developed [73]. This sensor was designed based on the formation of the AgNP/GQD hybrids following the attachment of Ag^+ onto the surface of

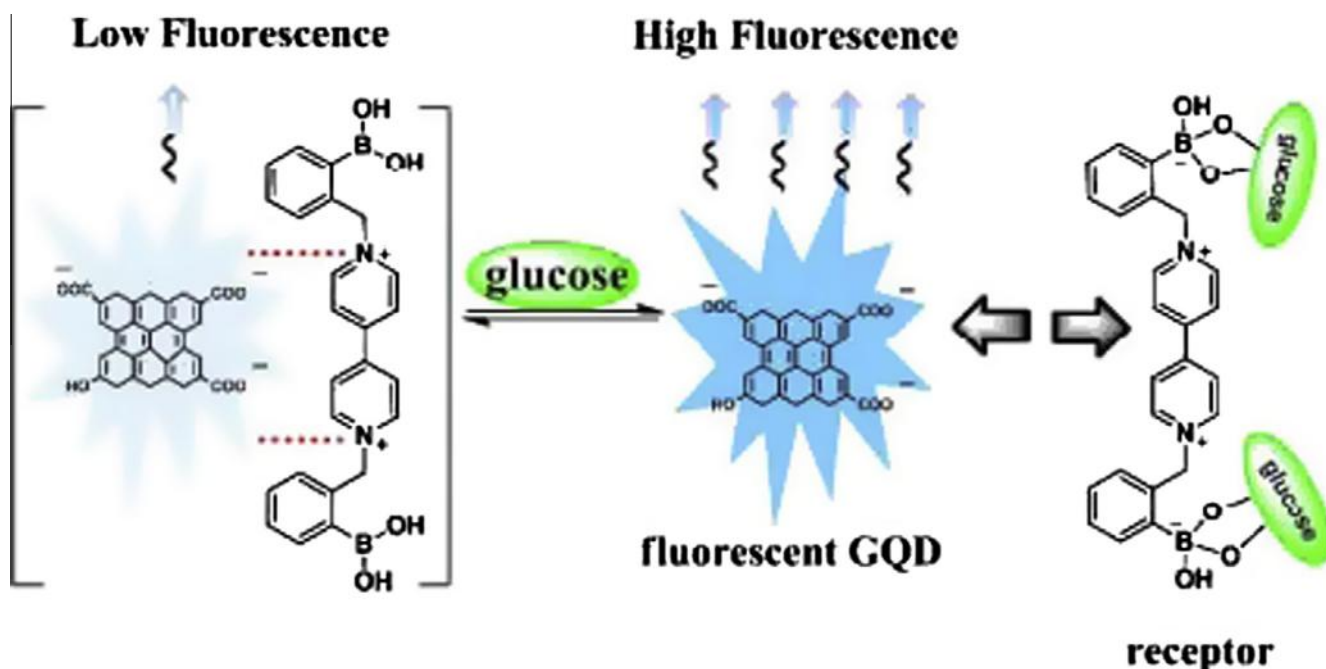


Fig. 24. Proposed glucose-sensing mechanism based on boronic acid-substituted bipyridinium salt (BBV) receptor and fluorescent graphene quantum dots (GQDs) [70].

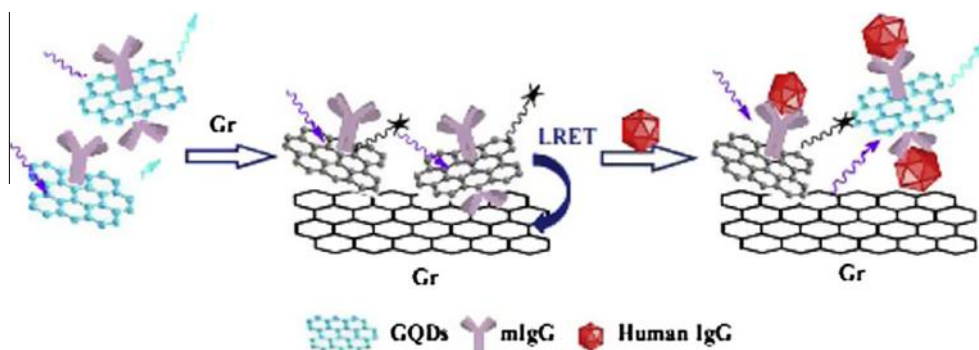


Fig. 25. A universal immunosensing strategy based on regulation of the interaction between graphene and graphene quantum dots (GQDs) [72].

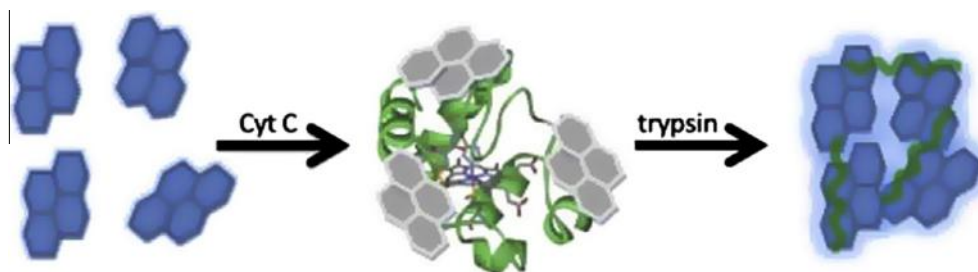


Fig. 26. The fluorescent biosensor for trypsin based on self-assembled graphene quantum dots (GQDs) [76].

the GQDs via electrostatic interaction. In the process, the addition of biothiols caused a further turn-off phenomenon through the formation of an Ag-S bond, unlike the turn-on sensor reported for carbon dots [74]. This label-free assay for the detection of Ag^+ and biothiols

was developed with an LOD of 3.5 nM for Ag^+ , 6.2 nM for Cys, 4.5 nM for Hcy and 4.1 nM for GSH in the range 0–100 nM.

Also, due to the excellent conductivity of GQDs, an electrochemical biosensor using a GQD-modified pyrolytic graphite electrode

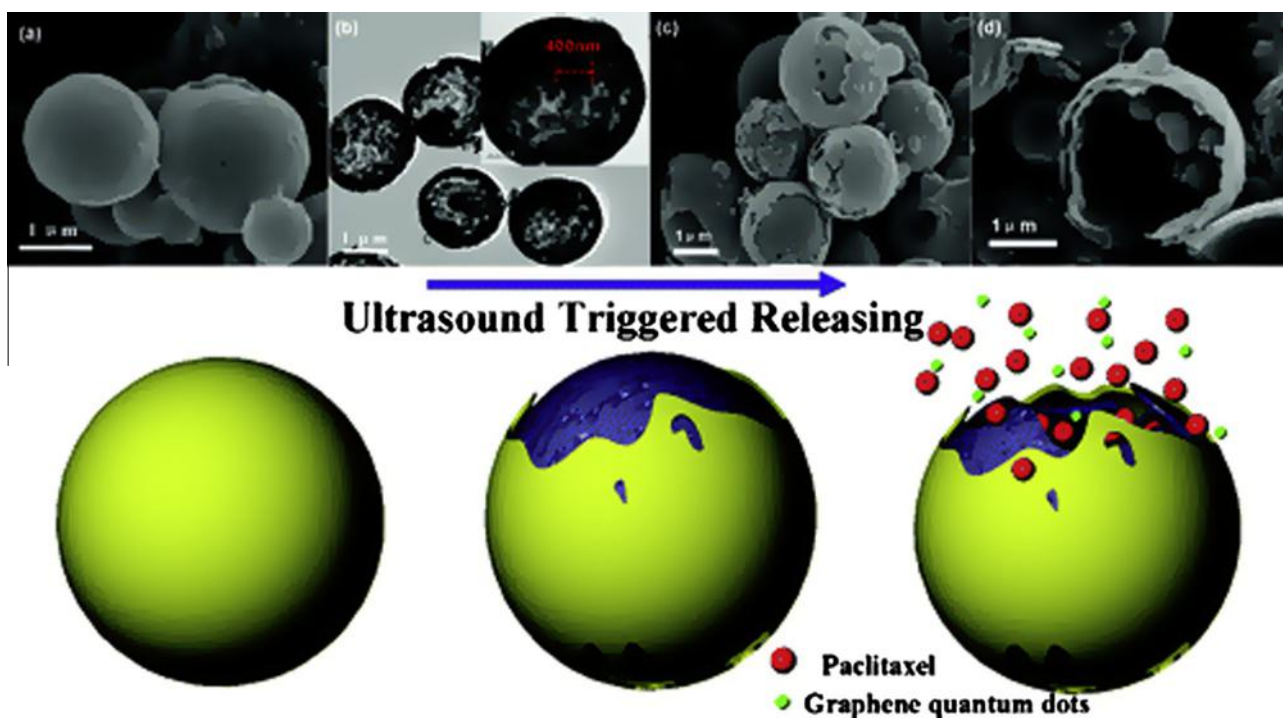


Fig. 27. (a) Scanning electron microscopy (SEM) image of trigger-released capsules; (b) transmission electron microscopy (TEM) image (the insert is a magnification of a single capsule); (c) SEM image of the capsules after ultrasound treatment for 5 min and (d) SEM image after ultrasound treatment for 15 min; and, (e) the procedures involved in shell cracking until drug release from the capsules with increasing ultrasound time [77].

coupled with specific sequence single-stranded DNA (ssDNA) as a probe was based on the strong interaction between ssDNA and graphene material [75]. Because of the inhibition of the electron transfer between the electrode and the electrochemically-active species $[\text{Fe}(\text{CN})_6]^{3-/4-}$ via electrostatic repulsion by ssDNA, the peak current of $[\text{Fe}(\text{CN})_6]^{3-/4-}$ evidently decreased. When the target molecules were present in the test solution, the peak current of $[\text{Fe}(\text{CN})_6]^{3-/4-}$ increased. The electrochemical sensor was flexible enough to be used to detect target molecules, such as ssDNA and protein.

Further, a biosensor for trypsin detection was designed on the basis that cytochrome c (Cyt c, rich in Fe^{3+}) induced remarkable fluorescence in self-assembled GQDs (Fig. 26) [76]. However, the special coordinate interaction between Fe^{3+} and the phenolic hydroxyl group of the GQDs (proved previously) could bind to the GQDs using electrostatic interactions and completely quenched the fluorescence of GQDs through electron transfer. When trypsin was present, Cyt c cleaved into smaller fragments on the c-terminal side of arginine and lysine residues, and the Fe^{3+} in Cyt c was possibly reduced to Fe^{2+} using a digestive enzyme. However, the trypsin-cleaved peptide bonds of Cyt c to the lysine and arginine residues could reduce the GQDs into reducing-GQDs and, as a result, the fluorescence of the GQDs was restored. This label-free, fluorescence-enhanced sensor is sensitive and selective to trypsin with an LOD of 33 ng mL^{-1} .

4.2.2. Drug release

A multifunctional core-shell capsule platform for simultaneous fluorescence imaging, magnetically-guided delivery, and ultrasound-triggered releasing has been produced [77]. As illustrated in Fig. 27, the platform comprised olive oil as the reservoir of the oil-soluble drug. GQDs were taken as an optical information indicator for *in-situ* monitoring of the drug release; Fe_3O_4 was used as a magnetic targeting drug carrier and a dual-layer porous titania shell was applied as a sensitive vehicle. The drug paclitaxel was released when the dual layer of the titania shell cracked under ultrasound stimulation, and the profile could be controlled by the frequency of the ultrasound. The Fe_3O_4 and GQDs functioned successfully for magnetic targeting and fluorescence imaging, respectively. Furthermore, we expect the results to play a significant role in the development of controlled-release drugs and delivery of water-insoluble drugs.

4.2.3. DNA cleavage

To explore the applicability of GQDs, a novel DNA-cleavage system using GQDs and copper ions was inspired by the fact that GO can be intercalated into DNA, and experimental results that proved that $\text{GQD}/\text{Cu}^{2+}$ could cleave the DNA molecules more efficiently than GO/Cu^{2+} at the same concentration [39]. The exploration of the detailed cleavage mechanism, optimization of cleavage conditions, and identification of the cleavage products confirmed that

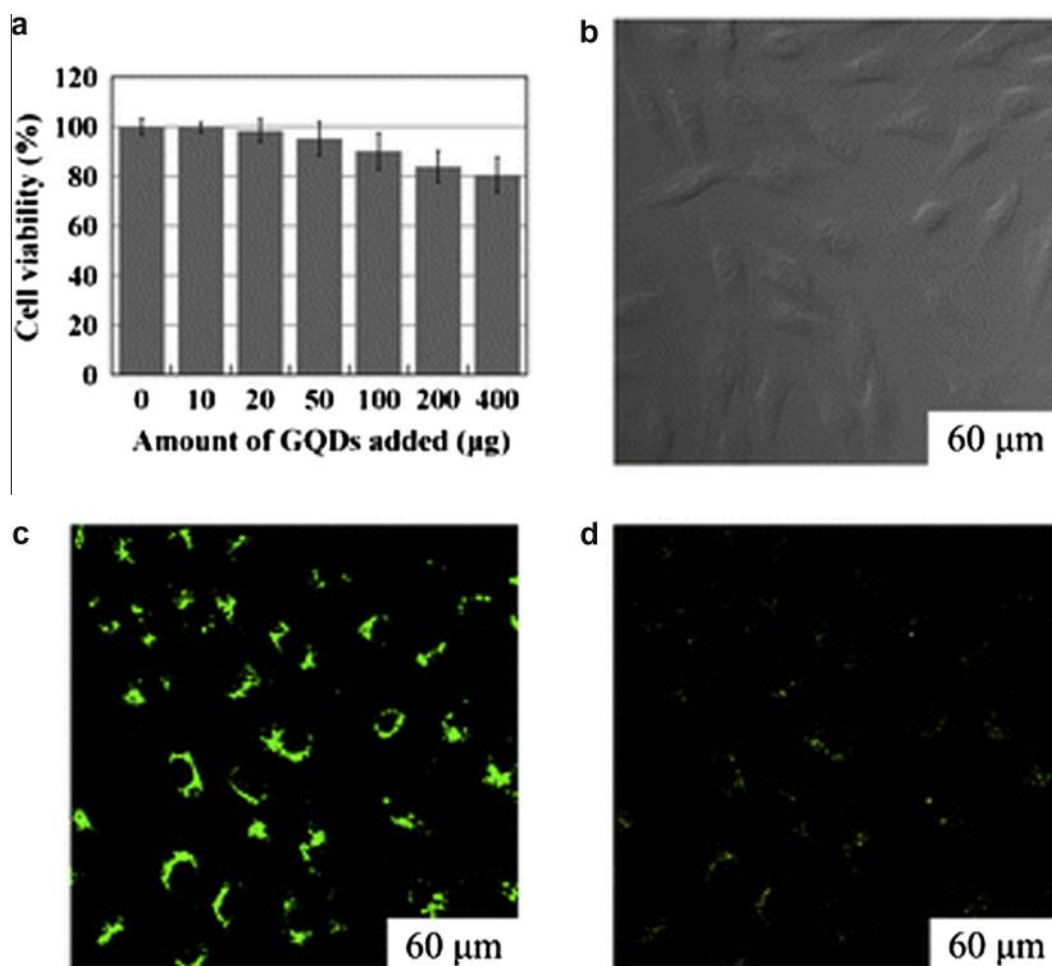


Fig. 28. Cellular toxicity and cellular imaging of graphene quantum dots (GQDs). (a) Effect of GQDs on viability of MG-63 cells; (b), (c) and (d) are washed cells imaged under bright field, 405 nm and 488 nm excitations, respectively.

GQD interaction with DNA is much stronger than that of the μm -sized GO sheets.

These interesting results open the way to further potential applications of GQDs in biological and medical research.

4.2.4. Bioimaging

The biological imaging of semiconductor QDs has been greatly limited by the intrinsic toxicity of the semiconductor QDs. Since GQDs provide physiological stability, low cytotoxicity and an eco-friendly nature, they are promising candidates for semiconductor QDs for bioimaging applications. *In-vitro* cellular studies were performed with green GQDs in human breast cancer cell lines T47D [30]. Fluorescent images clearly show the phase contrast image of T47D cells, the nucleus stained blue with 4,6-diamino-2-phenyl indole (DAPI), and with an agglomerated high contrast fluorescent image of green GQDs around each nucleus, and overlaying the image of the cell with phase contrast, DAPI and gGQDs. Stem cells, neurosphere cells (NSCs), pancreas progenitor cells (PPCs) and cardiac progenitor cells (CPCs) were incubated with GQDs at a concentration of 25 mg mL^{-1} for 24 h at 37°C [55]. After being washed three times with phosphate buffer solution and fixed with 4% paraformaldehyde for 20 min at room temperature, confocal fluorescent images of the three types of stem cell (with an excitation wavelength of 405 nm) clearly revealed the morphology of the cells with their internalized GQDs due to the clear observation of PL spots in the cytoplasmic area of these stem cells and relatively weak PL at the central region of the nucleus. This result also confirmed that GQDs easily penetrate into the stem cells but do not enter the nuclei. Furthermore, after several runs of repeated excitation, no intensity change of the fluorescence could be detected in the microscopy images, indicating high photostability of the GQDs in the cells. Even adding 400 mg of GQDs to 150 mL of culture medium (104 cells) did not decrease the cell activity significantly in 3-(4,5-dimethylthiazol-2-yl)-2,5-diphenyltetrazolium bromide (MTT) assay (Fig. 28a) [35]. Confocal fluorescence microscope images showed a bright green area inside the cells, indicating translocation of GQDs through the cell membrane (405 nm excitation) (Fig. 28b and c). When the excitation wavelength changed to 488 nm, a green–yellow color could be observed (Fig. 28d). These results indicated that GQDs could be used in bioimaging and other biomedical applications, even when involving high cell concentrations.

5. Summary and outlook

As presented above, GQDs, as a new graphene-based nanomaterial, have inspired intensive research in environmental, biological and other fields because of their low cytotoxicity, excellent stability and resilience of PL *in vivo*. There are many available methods for preparing GQDs, which have special properties, such as absorption, PL and electroluminescence, which can be obtained by monitoring the band gap with unique size-tuning and functional-modification methods.

However, some issues remain for further studies:

- (1) understanding the PL properties of GQDs is still poor, although, to date, some possible mechanisms have been proposed, such as size effect, surface modification, and doping with other elements;
- (2) the mechanisms deduced from the optical properties of the GQDs generated vary, so a study of the detailed mechanism for PL in GQDs would be highly significant;
- (3) exploration of the preparation of high-quality GQDs with uniform size and morphology is still ongoing;

- (4) since the GQDs derived from large graphene-based materials are heterogeneous in size and morphology, we expected that GQDs will be obtained from small molecules via appropriate methods of synthesis;
- (5) in spite of the achievement of GQDs with different colored PL properties, including PL in the near-infrared region, the quantum yields of most GQDs are still lower than 20%, so the improvement of GQDs is imperative because of their restricted application in many fields arising from their lower quantum yields.
- (6) metal-enhanced fluorescence may be considered for quantum-yield enhancement and a study has proved its feasibility [78]; and, last but not least,
- (7) compared with the environmental applications of GQDs, more studies concerning the application of GQDs in bioanalysis and the energy-related field are needed.

There is no doubt that new strategies for surface modification need to be developed for application in analysis. With their uniform size, excellent PL and high quantum yields, GQDs will no doubt be used in more creative applications.

Acknowledgments

This research work was financially supported by the National Nature Scientific Foundation of China (No. 21175112, No. 21375112) and NFFTS (No. J1030415), which are gratefully acknowledged. Furthermore, we would like to extend our thanks to Professor John Hodgkiss of The University of Hong Kong for his assistance with English.

References

- [1] R. Bakry, R.M. Vallant, M. Najam-ul-Haq, M. Rainer, Z. Szabo, C.W. Huck, G.K. Bonn, Medicinal applications of fullerenes, *Int. J. Nanomed.* 2 (2007) 639–649.
- [2] D.M. Guldi, B.M. Illescas, C.M. Atienza, M. Wielopolski, N. Martin, Fullerene for organic electronics, *Chem. Soc. Rev.* 38 (2009) 1587–1597.
- [3] M.F. De Volder, S.H. Tawfik, R.H. Baughman, A.J. Hart, Carbon nanotubes: present and future commercial applications, *Science* 339 (2013) 535–539.
- [4] S. Park, M. Vosguerichian, Z. Bao, A review of fabrication and applications of carbon nanotube film-based flexible electronics, *Nanoscale* 5 (2013) 1727–1752.
- [5] M. Terrones, Science and technology of the twenty-first century: synthesis, properties, and applications of carbon nanotubes, *Annu. Rev. Mater. Res.* 33 (2003) 419–501.
- [6] A.K. Geim, Graphene: status and prospects, *Science* 324 (2009) 1530–1534.
- [7] X. Huang, Z. Yin, S. Wu, X. Qi, Q. He, Q. Zhang, Q. Yan, F. Boey, H. Zhang, Graphene-based materials: synthesis, characterization, properties, and applications, *Small* 7 (2011) 1876–1902.
- [8] J. Yao, Y. Sun, M. Yang, Y. Duan, Chemistry, physics and biology of graphene-based nanomaterials: new horizons for sensing, imaging and medicine, *J. Mater. Chem.* 22 (2012) 14313–14329.
- [9] C. Chung, Y.-K. Kim, D. Shin, S.-R. Ryoo, B.H. Hong, D.H. Min, Biomedical applications of graphene and graphene oxide, *Accounts Chem. Res.* 46 (2013) 2211–2224.
- [10] V. Georgakilas, M. Otyepka, A.B. Bourlinos, V. Chandra, N. Kim, K.C. Kemp, P. Hobza, R. Zboril, K.S. Kim, Functionalization of graphene: covalent and non-covalent approaches, derivatives and applications, *Chem. Rev.* 112 (2012) 6156–6214.
- [11] S. Fujii, T. Enoki, Cutting of oxidized graphene into nanosized pieces, *J. Am. Chem. Soc.* 132 (2010) 10034–10041.
- [12] X. Li, X. Wang, L. Zhang, S. Lee, H. Dai, Chemically derived, ultrasmooth graphene nanoribbon semiconductors, *Science* 319 (2008) 1229–1232.
- [13] L.A. Ponomarenko, F. Schedin, M.I. Katsnelson, R. Yang, E.W. Hill, K.S. Novoselov, A.K. Geim, Chaotic dirac billiard in graphene quantum dots, *Science* 320 (2008) 356–358.
- [14] K.A. Ritter, J.W. Lyding, The influence of edge structure on the electronic properties of graphene quantum dots and nanoribbons, *Nat. Mater.* 8 (2009) 235–242.
- [15] D.Y. Pan, J.C. Zhang, Z. Li, M.H. Wu, Hydrothermal route for cutting graphene sheets into blue-luminescent graphene quantum dots, *Adv. Mater.* 22 (2010) 734–738.
- [16] H. Cheng, Y. Zhao, Y. Fan, X. Xie, L. Qu, G. Shi, Graphene-quantum-dot assembled nanotubes: a new platform for efficient raman enhancement, *ACS Nano* 6 (2012) 2237–2244.

- [17] J. Shen, Y. Zhu, X. Yang, C. Li, Graphene quantum dots: emergent nanolights for bioimaging, sensors, catalysis and photovoltaic devices, *Chem. Commun.* 48 (2012) 3686–3699.
- [18] Z. Zhang, J. Zhang, N. Chen, L. Qu, Graphene quantum dots: an emerging material for energy-related applications and beyond, *Energy Environ. Sci.* 5 (2012) 8869–8890.
- [19] S. Zhu, S. Tang, J. Zhang, B. Yang, Control the size and surface chemistry of graphene for the rising fluorescent materials, *Chem. Commun. (Camb.)* 48 (2012) 4527–4539.
- [20] H. Tetsuka, R. Asahi, A. Nagoya, K. Okamoto, I. Tajima, R. Ohta, A. Okamoto, Optically tunable amino-functionalized graphene quantum dots, *Adv. Mater.* 24 (2012) 5333–5338.
- [21] P.H. Luo, Z. Ji, C. Li, G. Shi, Aryl-modified graphene quantum dots with enhanced photoluminescence and improved pH tolerance, *Nanoscale* 5 (2013) 7361–7367.
- [22] J.H. Shen, Y.H. Zhu, C. Chen, X.L. Yang, C.Z. Li, Facile preparation and upconversion luminescence of graphene quantum dots, *Chem. Commun.* 47 (2011) 2580–2582.
- [23] J. Shen, Y. Zhu, X. Yang, J. Zong, J. Zhang, C. Li, One-pot hydrothermal synthesis of graphene quantum dots surface-passivated by polyethylene glycol and their photoelectric conversion under near-infrared light, *New J. Chem.* 36 (2012) 97–101.
- [24] S.H. Jin, D.H. Kim, G.H. Jun, S.H. Hong, S. Jeon, Tuning the photoluminescence of graphene quantum dots through the charge transfer effect of functional groups, *ACS Nano* 7 (2013) 239–245.
- [25] Y. Li, Y. Zhao, H.H. Cheng, Y. Hu, G.Q. Shi, L.M. Dai, L.T. Qu, Nitrogen-doped graphene quantum dots with oxygen-rich functional groups, *J. Am. Chem. Soc.* 134 (2012) 15–18.
- [26] C. Hu, Y. Liu, Y. Yang, J. Cui, Z. Huang, Y. Wang, L. Yang, H. Wang, Y. Xiao, J. Rong, One-step preparation of nitrogen-doped graphene quantum dots from oxidized debris of graphene oxide, *J. Mater. Chem. B* 1 (2013) 39–42.
- [27] M. Li, W. Wu, W. Ren, H.-M. Cheng, N. Tang, W. Zhong, Y. Du, Synthesis and upconversion luminescence of N-doped graphene quantum dots, *Appl. Phys. Lett.* 101 (2012), 103107–1–3.
- [28] Q. Feng, Q. Cao, M. Li, F. Liu, N. Tang, Y. Du, Synthesis and photoluminescence of fluorinated graphene quantum dots, *Appl. Phys. Lett.* 102 (2013), 013111–1–3.
- [29] J. Lu, P.S.E. Yeo, C.K. Gan, P. Wu, K.P. Loh, Transforming C_{60} molecules into graphene quantum dots, *Nat. Nanotechnology* 6 (2011) 247–252.
- [30] J. Peng, W. Gao, B.K. Gupta, Z. Liu, R. Romero-Aburto, L.H. Ge, L. Song, L.B. Alemany, X.B. Zhan, G.H. Gao, S.A. Vithayathil, B.A. Kaiparettu, A.A. Marti, T. Hayashi, J.J. Zhu, P.M. Ajayan, Graphene quantum dots derived from carbon fibers, *Nano Lett.* 12 (2012) 844–849.
- [31] M. Nurunnabi, Z. Khatun, G.R. Recek, D.Y. Lee, Y.K. Lee, Near infra-red photoluminescent graphene nanoparticle greatly expands use in noninvasive biomedical imaging, *Chem. Commun.* 49 (2013) 5079–5081.
- [32] Y. Dong, C. Chen, X. Zheng, L. Gao, Z. Cui, H. Yang, C. Guo, Y. Chi, C. Li, One-step and high yield simultaneous preparation of single- and multi-layer graphene quantum dots from CX-72 carbon black, *J. Mater. Chem.* 22 (2012) 8764–8766.
- [33] J. Lu, J. Yang, J. Wang, A. Lim, S.W.K.P. Loh, One-pot synthesis of fluorescent carbon nanoribbons, nanoparticles, and graphene by the exfoliation of graphite in ionic liquids, *ACS Nano* 3 (2009) 2367–2375.
- [34] D.B. Shinde, V.K. Pillai, Electrochemical preparation of luminescent graphene quantum dots from multiwalled carbon nanotubes, *Chem. Eur. J.* 18 (2012) 12522–12528.
- [35] S. Zhu, J. Zhang, C. Qiao, S. Tang, Y. Li, W. Yuan, B. Li, L. Tian, F. Liu, R. Hu, H. Gao, H. Wei, H. Zhang, H. Sun, B. Yang, Strongly green-photoluminescent graphene quantum dots for bioimaging applications, *Chem. Commun.* 47 (2011) 6858–6860.
- [36] S. Chen, J.W. Liu, M.L. Chen, X.W. Chen, J.H. Wang, Unusual emission transformation of graphene quantum dots induced by self-assembled aggregation, *Chem. Commun.* 48 (2012) 7637–7639.
- [37] L. Li, J. Ji, R. Fei, C. Wang, Q. Lu, J. Zhang, L. Jiang, J. Zhu, A facile microwave avenue to electrochemiluminescent two-color graphene quantum dots, *Adv. Funct. Mater.* 22 (2012) 2971–2979.
- [38] L.X. Lin, S.W. Zhang, Creating high yield water soluble luminescent graphene quantum dots via exfoliating and disintegrating carbon nanotubes and graphite flakes, *Chem. Commun.* 48 (2012) 10177–10179.
- [39] X. Zhou, Y. Zhang, Chong Wang, X. Wu, Y. Yang, H. Wu, S. Guo, Photo-fenton reaction of graphene oxide: a new strategy to prepare graphene quantum dots for DNA cleavage, *ACS Nano* 6 (2012) 6592–6599.
- [40] T. Gokus, R.R. Nair, A. Bonetti, M.B. Hmler, A. Lombardo, K.S. Novoselov, A.K. Geim, A. Hartschuh, A.C. Ferrari, Making graphene luminescent by oxygen plasma treatment, *ACS Nano* 3 (2009) 3963–3968.
- [41] J. Lee, K. Kim, W.I. Park, B.H. Kim, J.H. Park, T.H. Kim, S. Bong, C.H. Kim, G. Chae, M. Jun, Y. Hwang, Y.S. Jung, S. Jeon, Uniform graphene quantum dots patterned from self-assembled silica nanodots, *Nano Lett.* 12 (2012) 6078–6083.
- [42] L. Tang, R. Ji, X. Cao, J. Lin, H. Jiang, X. Li, K.S. Teng, C.M. Luk, S. Zeng, J. Hao, S.P. Lau, Deep ultraviolet photoluminescence of water-soluble self-passivated graphene quantum dots, *ACS Nano* 6 (2012) 5102–5110.
- [43] Y. Dong, J. Shao, C. Chen, H. Li, R. Wang, Y. Chi, X. Lin, G. Chen, Blue luminescent graphene quantum dots and graphene oxide prepared by tuning the carbonization degree of citric acid, *Carbon* 50 (2012) 4738–4743.
- [44] R.L. Liu, D.Q. Wu, X.L. Feng, K. Mullen, Bottom-up fabrication of photoluminescent graphene quantum dots with uniform morphology, *J. Am. Chem. Soc.* 133 (2011) 15221–15223.
- [45] X. Wu, F. Tian, W. Wang, J. Chen, M. Wu, J. Lia, X. Zhao, Fabrication of highly fluorescent graphene quantum dots using L-glutamic acid for in vitro/in vivo imaging and sensing, *Nanoscale* 1 (2013) 4676–4684.
- [46] L. Li, X. Yan, Colloidal graphene quantum dots, *Phys. Chem. Lett.* 1 (2010) 2572–2576.
- [47] F. Jiang, D. Chen, R. Li, Y. Wang, G. Zhang, S. Li, J. Zheng, N. Huang, Y. Gu, C. Shu, Eco-friendly synthesis of size-controllable amine-functionalized graphene quantum dots with antimycoplasma property, *Nanoscale* 5 (2013) 1137–1142.
- [48] S. Zhu, J. Zhang, S. Tang, C. Qiao, L. Wang, H. Wang, X. Liu, B. Li, Y. Li, W. Yu, X. Wang, H. Sun, B. Yang, Surface chemistry routes to modulate the photoluminescence of graphene quantum dots: from fluorescence mechanism to up-conversion bioimaging applications, *Adv. Funct. Mater.* 12 (2012) 4732–4740.
- [49] Y. Wang, Y. Shao, D.W. Matson, J. Li, Y. Lin, Nitrogen-doped graphene and its application in electrochemical biosensing, *ACS Nano* 4 (2010) 1790–1798.
- [50] X. Wang, X. Li, L. Zhang, Y. Yoon, P.K. Weber, H. Wang, J. Guo, H. Dai, N-doping of graphene through electrothermal reactions with ammonia, *Science* 324 (2009) 768–771.
- [51] Y. Xue, J. Liu, H. Chen, R. Wang, D. Li, J. Qu, L. Dai, Nitrogen-doped graphene foams as metal-free counter electrodes in high-performance dye-sensitized solar cells, *Angew. Chem. Int. Ed. Engl.* 51 (2012) 12124–12127.
- [52] Q.Q. Li, S. Zhang, L.M. Dai, L.S. Li, Nitrogen-doped colloidal graphene quantum dots and their size-dependent electrocatalytic activity for the oxygen reduction reaction, *J. Am. Chem. Soc.* 134 (2012) 18932–18935.
- [53] K.J. Jeon, Z. Lee, E. Pollak, L. Moreschini, A. Bostwick, C.M. Park, R. Mendelsberg, V. Radmilovic, R. Kostecki, T.J. Richardson, E. Rotenberg, Fluorographene: a wide bandgap semiconductor with ultraviolet luminescence, *ACS Nano* 5 (2011) 1042–1046.
- [54] J.T. Robinson, J.S. Burgess, C.E. Junkermeier, S.C. Badescu, T.L. Reinecke, F.K. Perkins, M.K. Zalalutdniov, J.W. Baldwin, J.C. Culbertson, P.E. Sheehan, E.S. Snow, Properties of fluorinated graphene films, *Nano Lett.* 10 (2010) 3001–3005.
- [55] M. Zhang, L. Bai, W. Shang, W. Xie, H. Ma, Y. Fu, D. Fang, H. Sun, L. Fan, M. Han, C. Liu, S. Yang, Facile synthesis of water-soluble, highly fluorescent graphene quantum dots as a robust biological label for stem cells, *J. Mater. Chem.* 22 (2012) 7461–7467.
- [56] S. Zhu, J. Zhang, X. Liu, B. Li, X. Wang, S. Tang, Q. Meng, Y. Li, C. Shi, R. Hu, B. Yang, Graphene quantum dots with controllable surface oxidation, tunable fluorescence and up-conversion emission, *RSC Adv.* 2 (2012) 2717–2720.
- [57] Y. Sun, S. Wang, C. Li, P. Luo, L. Tao, Y. Wei, G. Shi, Large scale preparation of graphene quantum dots from graphite with tunable fluorescence properties, *Phys. Chem. Chem. Phys.* 15 (2013) 9907–9913.
- [58] F. Yang, M. Zhao, B. Zheng, D. Xiao, L. Wu, Y. Guo, Influence of pH on the fluorescence properties of graphene quantum dots using ozonation pre-oxide hydrothermal synthesis, *J. Mater. Chem.* 22 (2012) 25471–25481.
- [59] S. Zhuo, M. Shao, S. Lee, Upconversion and downconversion fluorescent graphene quantum dots: ultrasonic preparation and photocatalysis, *ACS Nano* 6 (2012) 1059–1064.
- [60] K. Gong, F. Du, Z. Xia, M. Durstock, L. Dai, Nitrogen-doped carbon nanotube arrays with high electrocatalytic activity for oxygen reduction, *Science* 323 (2009) 760–764.
- [61] L. Qu, Y. Liu, J.-B. Baek, L. Dai, Nitrogen-doped graphene as efficient metal-free electrocatalyst for oxygen reduction in fuel cells, *ACS Nano* 4 (2010) 1321–1326.
- [62] K. Parvez, S.B. Yang, Y. Hernandez, A. Winter, A. Turchanin, X.L. Feng, K. Mullen, Nitrogen-doped graphene and its iron-based composite as efficient electrocatalysts for oxygen reduction reaction, *ACS Nano* 6 (2012) 9541–9550.
- [63] Y. Liu, P. Wu, Graphene quantum dot hybrids as efficient metal-free electrocatalyst for the oxygen reduction reaction, *ACS Appl. Mater. Interfaces* 5 (2013) 3362–3369.
- [64] L. Fan, Y. Hu, X. Wang, L. Zhang, F. Li, D. Han, Z. Li, Q. Zhang, Z. Wang, L. Niu, Fluorescence resonance energy transfer quenching at the surface of graphene quantum dots for ultrasensitive detection of TNT, *Talanta* 101 (2012) 192–197.
- [65] Y.Q. Dong, G.L. Li, N.N. Zhou, R.X. Wang, Y.W. Chi, G.N. Chen, Graphene quantum dot as a green and facile sensor for free chlorine in drinking water, *Anal. Chem.* 84 (2012) 8378–8382.
- [66] J.M. Bai, L. Zhang, R.P. Liang, J.D. Qiu, Graphene quantum dots combined with europium ions as photoluminescent probes for phosphate sensing, *Chem. Eur. J.* 19 (2013) 3822–3826.
- [67] J.J. Liu, X.L. Zhang, Z.X. Cong, Z.T. Chen, H.H. Yang, G.N. Chen, Glutathione-functionalized graphene quantum dots as selective fluorescent probes for phosphate-containing metabolites, *Nanoscale* 5 (2013) 1810–1815.
- [68] D. Wang, L. Wang, X. Dong, Z. Shi, J. Jin, Chemically tailoring graphene oxides into fluorescent nanosheets for Fe^{3+} ion detection, *Carbon* 50 (2012) 2147–2154.
- [69] Y. Zhang, C. Wu, X. Zhou, X. Wu, Y. Yang, H. Wu, S. Guo, J. Zhang, Graphene quantum dots/gold electrode and its application in living cell H_2O_2 detection, *Nanoscale* 5 (2013) 1816–1819.
- [70] Y.H. Li, L. Zhang, J. Huang, R.P. Liang, J.D. Qiu, Fluorescent graphene quantum dots with a boronic acid appended bipyridinium salt to sense monosaccharides in aqueous solution, *Chem. Commun.* 49 (2013) 5180–5182.
- [71] H. Razmi, R. Mohammad-Rezaei, Graphene quantum dots as a new substrate for immobilization and direct electrochemistry of glucose oxidase: application to sensitive glucose determination, *Biosens. Bioelectron.* 41 (2013) 498–504.
- [72] H.M. Zhao, Y.Y. Chang, M. Liu, S. Gao, H.T. Yu, X. Quan, A universal immunosensing strategy based on regulation of the interaction between graphene and graphene quantum dots, *Chem. Commun.* 49 (2013) 234–236.

- [73] X. Ran, H. Sun, F. Pu, J. Ren, X. Qu, Ag nanoparticles-decorated graphene quantum dots for label-free, rapid and sensitive detection of Ag⁺ and biothiols, *Chem. Commun.* 49 (2012) 1079–1081.
- [74] L. Zhou, Y.H. Lin, Z.Z. Huang, J.S. Ren, X.G. Qu, Carbon nanodots as a fluorescence probes for rapid, sensitive, and label-free detection of Hg²⁺ and biothiols in complex matrices, *Chem. Commun.* 48 (2012) 1147–1149.
- [75] J. Zhao, G. Chen, L. Zhu, G. Li, Graphene quantum dots-based platform for the fabrication of electrochemical biosensors, *Electrochem. Commun.* 13 (2011) 31–33.
- [76] X. Li, S. Zhu, B. Xu, K. Ma, J. Zhang, B. Yang, W. Tian, Self-assembled graphene quantum dots induced by cytochrome c: a novel biosensor for trypsin with remarkable fluorescence enhancement, *Nanoscale* 5 (2013) 7776–7779.
- [77] Y.J. Jing, Y.H. Zhu, X.L. Yang, J.H. Shen, C.Z. Li, Ultrasound-triggered smart drug release from multifunctional core-shell capsules one-step fabricated by coaxial electrospray method, *Langmuir* 27 (2011) 1175–1180.
- [78] L. Deng, L. Liu, C. Zhu, D. Li, S. Dong, Hybrid gold nanocube@silica@graphene-quantum-dot superstructures: synthesis and specific cell surface protein imaging applications, *Chem. Commun.* 49 (2013) 2503–2505.